Research Square

Preprints are preliminary reports that have not undergone peer review.
They should not be considered conclusive, used to inform clinical practice,
or referenced by the media as validated information.

Alkbh5a-mediated m6A methylation promotes seawater adaptation via chromatin remodeling and tonebpa1 activation in anadromous Oncorhynchus mykiss

Yuan Tian

tianyuan@ouc.edu.cn

Ocean University of China

Han Yu

Ocean University of China

Yiwen Sun

Ocean University of China

Manu Kumar Gundappa

University of Edinburgh

Ye Lu

Ocean University of China

Xiangbing Zeng

Ocean University of China

Boyuan Wang

Auburn University

Jinghong He

Ocean University of China

Huanhuan Zhu

Ocean University of China

Dan Li

Ocean University of China

Yang Qu

Ocean University of China

Chenghao Xin

Ocean University of China

Yining Yu

Shandong Marine Group LTD.

Xiangke Meng

Shandong Marine Group LTD.

Daniel Macqueen
University of Edinburgh https://orcid.org/0000-0001-8050-7722
Qinfeng Gao
Ocean University of China

Article

Keywords:

Posted Date: June 21st, 2026

DOI: https://doi.org/10.21203/rs.3.rs-9981738/v1

License: This work is licensed under a Creative Commons Attribution 4.0 International License.
Read Full License

Additional Declarations: There is **NO** Competing Interest.

Alkbh5a-mediated m^{6}A methylation promotes seawater adaptation via chromatin remodeling and *tonebpa1* activation in anadromous *Oncorhynchus mykiss*

Han Yu[1, #], Yiwen Sun[1, #], Manu Kumar Gundappa[2], Ye Lu[1], Xiangbing Zeng[1], Boyuan Wang[3], Jinghong He[1], Huanhuan Zhu[1], Dan Li[1], Yang Qu[1], Chenghao Xin[1], Yining Yu[4], Xiangke Meng[4], Daniel J. Macqueen[5, *], Qinfeng Gao[1, *], Yuan Tian[1, *]

[1] Key Laboratory of Mariculture, Ministry of Education, Ocean University of China, Qingdao, Shandong Province, China

[2] Animal Breeding and Genomics, Wageningen University & Research, Wageningen, The Netherlands

[3] Department of Biological Sciences, Auburn University, Auburn, AL, USA

[4] Shandong Marine Group LTD., Jinan, Shandong, China

[5] The Roslin Institute and Royal (Dick) School of Veterinary Studies, The University of Edinburgh, Midlothian, UK

[#]These authors contributed equally

*Correspondence: tianyuan@ouc.edu.cn; qfgao@ouc.edu.cn; daniel.macqueen@roslin.ed.ac.uk

Abstract:

Salmonids are renowned for their anadromous life cycle, involving migrations between freshwater and marine environments with dramatic changes in salinity. RNA m^6A methylation is well acknowledged as an epigenomic mark that regulates stress responses in eukaryotic species, yet with nothing known on its role in osmoregulatory adaptation in fishes. Here, multiple lines of evidence demonstrate that *alkbh5a* represents a master regulator of m^6A abundance in gill epithelium of anadromous *Oncorhynchus mykiss*, promoting adaptation to salinity following smoltification. Repression of *alkbh5a* results in hyper-methylated *histone H1.0B*, which enhances its translation efficiency via Reader protein Hnrnpab1. As a nucleosome linker, enhanced Histone H1.0B remodels chromatin accessibility, leading to upregulation of only one *tonebp* paralogue gene (*tonebpa1*). Importantly, *tonebpa1* is shown to be crucial for ionocyte proliferation in response to hyper-salinity and hyper-osmotic environments. Together, these findings reveal novel epigenomic and molecular drivers of salinity adaptation that prepare salmonids for their seaward migration.

1. Introduction

Migratory life history strategies are widespread among fishes, occurring at multiple temporal and spatial scales for the purpose of feeding and reproduction, representing an important driver of evolutionary diversity[1,2]. Among the more extreme examples, members of the salmonid family are renowned for their long-distance anadromous migrations between freshwater and marine environments, demanding mechanisms to control osmoregulatory stress[3]. Anadromy is an evolved trait in salmonids, whose ancestor had a purely freshwater life-cycle, which is still retained in members such as the graylings[4]. Within Salmoninae, anadromy evolved in the ancestor to *Salmo*, *Oncorhynchus*, *Salvelinus* and *Parahucho* and is thought to have promoted species diversification[5,6]. Therefore, this group of fishes developed adaptive strategies to maintain osmotic homeostasis when moving between radically divergent salinities environments, which may be shared across anadromous salmonids.

Before seaward migration, juvenile salmonids go through the parr-smolt transformation, also called smoltification. During this time, parr-adapted to freshwater stream habitats - transform into silver-colored smolts adapted to life in the open ocean[7–9]. Over the past few decades, our understanding of this transformation has considerably expanded at the morphological, behavioral, physiological, biochemical and molecular levels[8,10]. Nonetheless, little information is known about the underlying epigenetic drivers, especially at the level of RNA modifications.

N^6-methyladenosine (m^6A) is the most prevalent and conserved RNA epigenetic modification in eukaryotes. The deposition of m^6A onto RNAs is predominantly catalyzed by methyltransferase, first purified and characterized in the 1990s[11,12]. The recent discovery of demethylases, such as FTO and ALKBH5, has established m^6A as a reversible and dynamic

52 modification, underscoring further complexity and the functional significance of m^{6}A-
53 mediated regulation[13,14]. To date, m^{6}A functions have been shown to be involved in all aspects
54 of RNA regulation, including splicing, folding, stability, export, and translational efficiency[15].
55 These multifaceted roles are largely achieved by indispensable Reader proteins, forming an
56 additional layer in the control the RNA-protein interactions[16,17].

57 RNA m^{6}A modification is required for a growing list of stress-associated responses including
58 cold tolerance[18], hypoxia resistance[19], heat adaptation[20,21] and immune responses[22,23]. Recently,
59 m^{6}A-dependent regulatory mechanisms linked to salinity adaptation have been characterized
60 solely in plants. In *Arabidopsis*, the cumulative effects of altered m^{6}A deposition increases
61 salinity stress tolerance, achieved by stabilizing and upregulating the expression of positive
62 regulator genes[24,25]. In *Sorghum*, hyper-methylated m^{6}A modifications within mRNAs of
63 osmotic-stress responsive genes are thought to increase their stability, activating abscisic acid
64 signaling to support normal growth under salinity stress[26].

65 However, the role of m^{6}A modifications in salinity adaptation remains unexplored in animals,
66 including in the context of fish anadromy. Among the tissues showing specializations linked to
67 anadromy in salmonids, the gill epithelium is crucial for the maintenance of ionic homeostasis,
68 largely attributed to specialized ionocytes as the primary sites of ion exchange, driven by
69 Na^+/K^+ ATPase (*nka*) and ion transporter genes[27]. Here, we investigated the potential roles of
70 m^{6}A methylation in salinity adaptation within the gill epithelium of *Oncorhynchus mykiss*
71 (rainbow trout), a globally farmed cold-water species of vast economic importance[28] (FAO,
72 2025) and representative of anadromous salmonids. Our findings establish a robust causal link
73 between m^{6}A methylation and salinity adaptation, highlighting key roles for RNA epigenomic

regulation in supporting anadromous life history strategies.

2. Results

2.1 Demethylase *alkbh5a* regulates gill RNA m^{6}A methylation in response to salinity challenge

To explore the potential role of RNA m^{6}A methylation in salinity adaptation during the parr to smolt transformation, we firstly measured the ratio of m^{6}A/A in total poly(A)-tailed RNA isolated from gill epithelium of *O. mykiss* smolts at different salinities (Fig. 1a). A significant increase in m^{6}A/A ratios was observed under seawater conditions (Fig. 1b; Supplementary Fig. 1), reflecting enhanced global m^{6}A abundance. Elsewhere, m^{6}A methylation was shown to be reversibly regulated by RNA methyltransferases and demethylases[13,14]. To systematically determine candidate m^{6}A regulators, an exhaustive set of methyltransferase and demethylase orthologs were searched in the *O. mykiss* genome (Supplementary Fig. 2a). Orthologs for all known vertebrate m^{6}A regulators were identified, namely *mettl3*, *mettl14*, *mettl16*, *wtap*, *alkbh5* and *fto*. However, owing to the salmonid-specific whole genome duplication (WGD)[29,30], all were retained as duplicated pairs in Atlantic salmon (*Salmo salar*) and *O. mykiss* with evidence for pseudogenization of one copy of *mettl3* and *mettl16* (Fig. 1c). Comparing *O. mykiss* with other vertebrate species, we identified strong similarity at the level of primary amino acid sequences, 3D structures and functional domains (Supplementary Fig. 2b), indicating the conservation of m^{6}A regulators in salmonids.

Next, the expression of m^{6}A regulator genes, distinguishing the identified salmonid-specific paralogs (appended with ‘a’ or ‘b’ at the end of each ohnolog in a pair) (Supplementary Fig. 3), was quantified in gill epithelium of *O. mykiss* smolts challenged with gradually increasing

96 salinity. Differential regulation was observed only for *mettl3a* and *alkbh5a*, which were each
97 downregulated as salinity increased (Fig. 1d-e; Supplementary Fig. 4a). The same
98 downregulation to increasing salinity was observed in a gill epithelial cell line (RTgill-W1)
99 (Fig. 1f-g; Supplementary Fig. 4b). The protein abundance of Mettl3a and Alkbh5a was
100 likewise consistently lower at increased salinity, both *in vivo* and *in vitro* (Fig. 1h-i). To confirm
101 their importance for m^6A methylation, *mettl3a* and *alkbh5a* were separately overexpressed in
102 RTgill-W1 cells (Supplementary Fig. 4c). While this did not alter global m^6A abundance for
103 *mettl3a* (Fig. 1j), overexpression of *alkbh5* reduced global m^6A abundance dramatically (Fig.
104 1k).

105 Together, these findings suggest that the salmonid-specific *alkbh5a* ohnolog, encoding a
106 master m^6A demethylase, negatively regulates m^6A methylation in the gill epithelium of *O.*
107 *mykiss* smolts when faced with salinity changes mirroring the migration of smolts into seawater
108 environments.

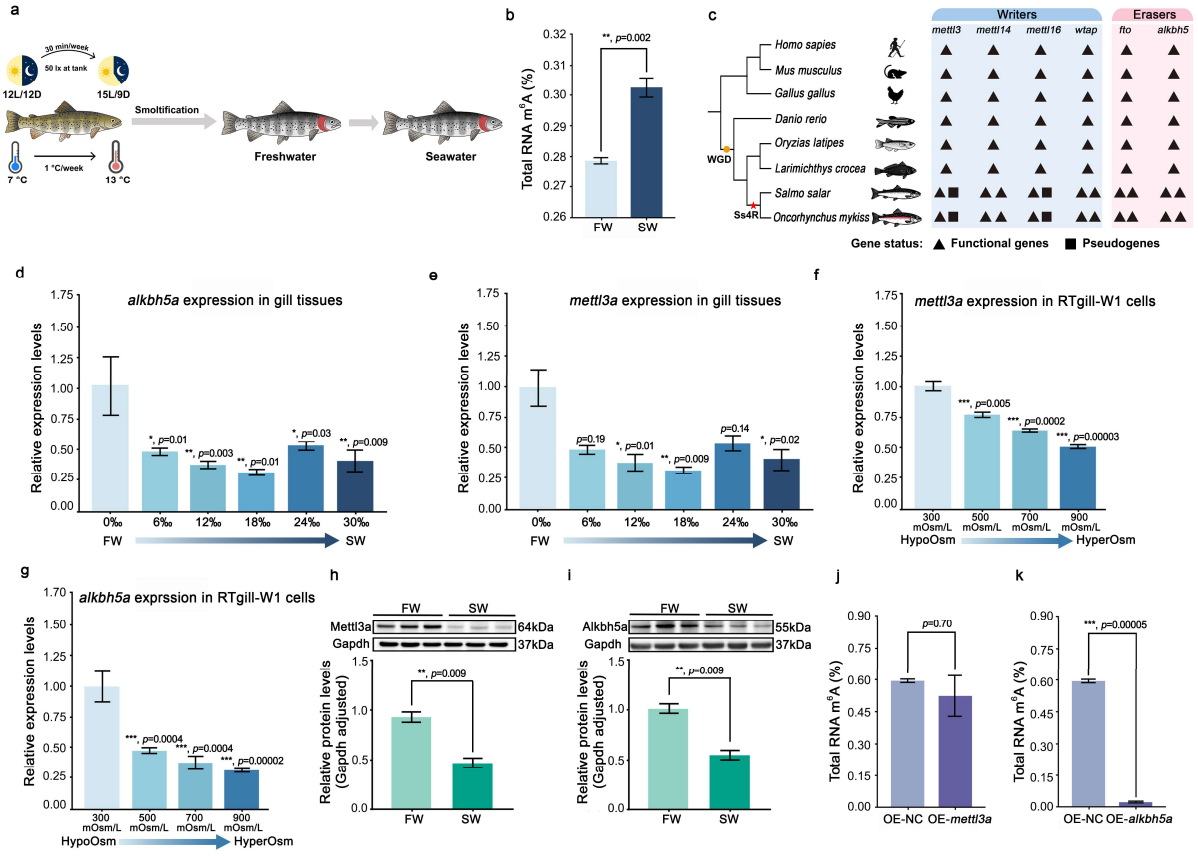


Fig. 1 Alkbh5a is a major regulator of m^{6}A methylation in the gill epithelium of *O. mykiss* smolts during salinity adaptation.

2.2 MeRIP-seq identifies *histone H1.0B* mRNA as a target for Alkbh5a demethylase

To more deeply explore the functional role of m^{6}A demethylase activity in salinity adaptation, we globally identified m^{6}A-containing mRNAs and quantified their methylation status using m^{6}A methylated RNA immunoprecipitation sequencing (MeRIP-seq), contrasting gill epithelium from freshwater (FW) and seawater (SW) groups. Altogether, 26,855 m^{6}A peaks were identified across 15,687 genes (43.18% of all genes) (Fig. 2a; Supplementary Data 1). At FDR < 0.05, 372 and 606 m^{6}A peaks were hypo- or hyper-methylated in SW vs. FW gills, respectively (Fig. 2b; Supplementary Data 2). Hyper-methylated peaks were enriched in m^{6}A

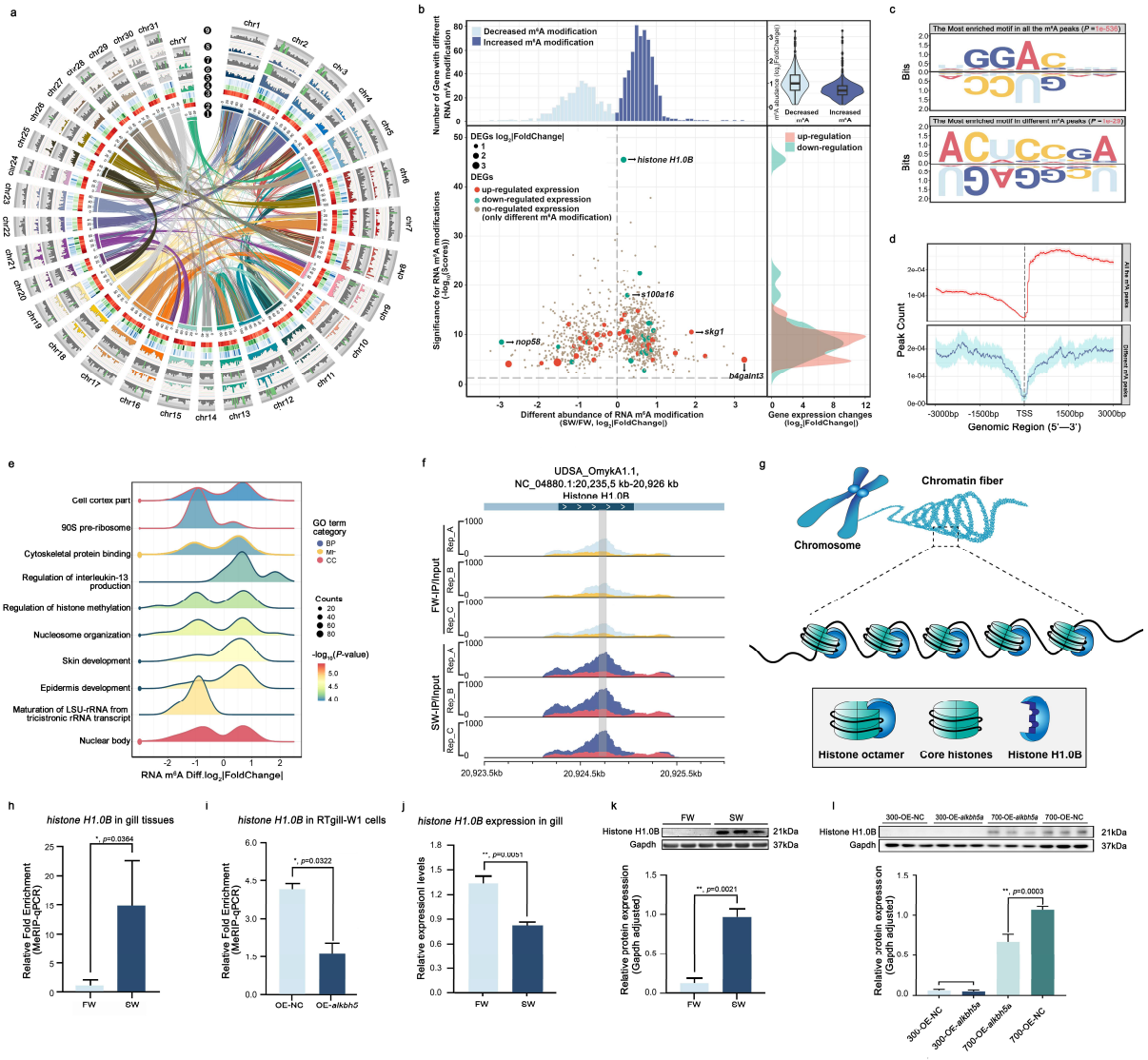
121 methylation sites (Fig. 2b). These results are consistent with the enhanced abundance of global
122 m^6A in gill epithelium of smolts in the SW group (Fig. 1b).

123 Integrating MeRIP-seq and RNA-seq revealed 37 up- and 21 down-regulated genes between
124 FW and SW groups that also showed hypo- or hyper-methylated m^6A peaks (Fig. 2b,
125 Supplementary Data 3). The expression accumulation of up-regulated genes seems to be similar
126 to those of down-regulated genes (Fig. 2b). There was no bias in expression response for genes
127 showing either hypo- or hyper-methylated m^6A peaks. The majority of m^6A peaks featured the
128 motif "UGGACUU" (Fig. 2c), analogous to the consensus m^6A "DRACH" motif (D, A/G/U;
129 R, A/G; and H, A/C/U) in mammals[31–33]. Conversely, the hypo- and hyper-methylated m^6A
130 peaks were enriched in the "ACUCCGA" motif (Fig. 2c). We further found that most m^6A sites
131 localized to gene bodies or untranslated regions (UTRs) (Fig. 2d).

132 Genes containing hypo- and hyper-methylated m^6A peaks showed strong enrichment in the
133 Gene Ontology (GO) term "nuclear body" (Fig. 2e), suggesting m^6A methylation regulates
134 nuclear genes in response to seawater challenge. Other enriched GO terms were linked to
135 epidermis development, protein synthesis and cytoskeleton regulation (Fig. 2e, Supplementary
136 Data 4). By scanning all the genes showing hypo- or hyper-methylated m^6A peaks, *histone*
137 *H1.0B* was distinguished by its high statistical significance, ~35 times above our statistical
138 cutoff (Fig. 2b; Fig. 2f-g). The strong enrichment of m^6A methylation for *histone H1.0B* in the
139 SW group was independently validated using MeRIP-qPCR (Fig. 2h; Supplementary Fig. 5).
140 Crucially, we also found that overexpression of *alkbh5a* strongly diminished the enrichment of
141 m^6A methylation on *histone H1.0B* (Fig. 2i), consistent with this gene being an important
142 substrate of Alkbh5a demethylase activity.

RNA-seq and RT-qPCR both indicated that *histone H1.0B* was slightly downregulated at the mRNA level in the SW group (Fig. 2j). In contrast, Histone H1.0B protein levels were significantly increased in the SW group (Fig. 2k). As m^6A methylation may impact mRNA translational efficiency[32,34], this discordance between mRNA expression and protein abundance could be explained by m^6A modification. To test this hypothesis, we overexpressed *alkbh5a* in RTgill-W1 cells under hyper-osmotic (700 mOsm/L) conditions, which led to reduced Histone H1.0B protein abundance (Fig. 2l; Supplementary Fig. 6). These results are consistent with repressed Alkbh5a demethylase activity in seawater enhancing m^6A methylation on *histone H1.0B* mRNA, increasing it translational efficiency.

Overall, because Histone H1.0B proteins play crucial roles in chromatin organization by facilitating the compaction of nucleosome arrays into higher order structures (Fig. 2g)[35,36], our results suggest that gill chromatin accessibility may be reshaped during salinity adaptation by m^6A-induced changes in *histone H1.0B* translation.



156

157 **Fig. 2 Transcriptome-wide signatures of m^{6}A methylation and identification of *histone***

158 ***H1.0 B* as an important substrate of Alkbh5a.**

159

160 **2.3 Hnrnpab1 identified as reader protein for m^{6}A methylation on *histone H1.0B* mRNA**

161 The broad effects of m^{6}A modification on mRNAs are governed by indispensable and highly

162 specific reader proteins. Hence, determining the reader protein for m^{6}A methylation on *histone*

163 *H1.0B* mRNA is required to determine whether and how this epigenetic mark regulates *histone*

164 *H1.0B* translation efficiency. RNA pull-down was performed using positive and negative m^{6}A

probes of *histone H1.0B* mRNA designed to harbor predicted hyper-methylation sites (Fig. 3a). Subsequent LC-MS/MS analysis revealed 991 proteins showing significant differences in abundance, pulled down by the m^{6}A probes (Supplementary Fig. 7a-d). As visualized in Fig. 3b (also see Supplementary Fig. 7e and Supplementary Data 5), these proteins were enriched for functions linked to translation and protein processing in the cytoplasm[37]. These data support our earlier inference that the translation of *histone H1.0B* mRNA is increased by m^{6}A methylation.

Several eukaryotic translation initiation factors were enriched among the pulled-down proteins, alongside ribosomal proteins (Fig. 3c). While previously reported to act as m^{6}A readers, translation initiation factors are thought to specifically bind to m^{6}A methylation in 5' UTRs in cap-independent manners, instead of regions near stop codons[38]. This prompted us to ask whether other m^{6}A reader proteins on *histone H1.0B* mRNA might be regulating translation by recruiting these translation initiation factors and ribosomal proteins. Hence, we manually checked all detected binding proteins showing different abundance between the negative and positive m^{6}A probes, to help identify candidate m^{6}A reader proteins. This approach failed to find any proteins encoded by YTH domain-containing genes, the most well-known eukaryotic m^{6}A readers[39]. However, a series of heterogeneous ribonucleoproteins (HnRNP) proteins were unexpectedly discovered with different abundance differences between negative and positive m^{6}A probes, which also shown elsewhere to act as m^{6}A readers with roles in RNA splicing[40], nuclear export[41], structure[42], stability[43] and translation[17] (Fig. 3d). Of them, *hnrnpab* was taken forward as our primary m^{6}A reader candidate in terms of its known roles in RNA translation [44] (Fig. 3d).

The hnRNPA/B family generally includes 5 gene members (*hnrnpab*, *hnrnapa0*, *hnrnpa1*, *hnrnpa2b1* and *hnrnpa3*), which shows marked variations in copy number across eukaryotic lineages[45,46]. However, most hnRNPA/B family members share a canonical RRM1 and RRM2 RNA binding domain arrangement (Fig. 3e). Further, several members of hnRNPABs harbor CBFNT and HnRNPA1 functional domains. Complete RRM1 and RRM2 domains are encoded by Hnrnpab proteins, providing structural evidence for conserved RNA recognition and binding functions (Fig. 3f). In *O. mykiss*, there are 4 different *hnrnpab* paralog genes due to additional teleost-specific and salmonid-specific whole genome duplication. Our LC-MS/MS results have identified Hnrnpab1 protein with abundance differences between negative and positive m^6A probes. Additionally, the docking analysis indicates that an m^6A residue at position 740 of *histone H1.0B* mRNA may be recognized and bound by Hnrnpab1 protein (Fig. 3f). The diversified surrounding residues (SER99, TRP100, THR102, SER103, LYS104, MET124 and GLY129) within the RRM1 domain was docked against *histone H1.0B* mRNA, resulting in predicted stereochemical interactions, including a precise van der Waals bond between Ser99 and m^6A methylation.

HnRNPAB proteins are generally located in the nucleus[47], inconsistent with the fact that translational regulation by m^6A readers usually occurs in the cytoplasm[48]. However, immunofluorescence staining in the gill epithelium of *O. mykiss* smolts revealed that Hnrnpab1 protein indeed accumulates specifically in the cytoplasm (Fig. 3g). To answer whether Hnrnpab1 shows m^6A reader activity, we carried out *hnrnpab1* gene knockdown in RTgill-W1 cells (Fig. 3h), following by RNA pull-down. Knockdown reduced the abundance of Histone H1.0B protein, consistent with lower translational efficiency (Fig. 3i).

Collectively, these data indicate that hnrnpab1 acts as an m^{6}A reader protein that enhances the translation efficiency of *histone H1.0B* mRNA in gill epithelium of *O. mykiss* smolts.

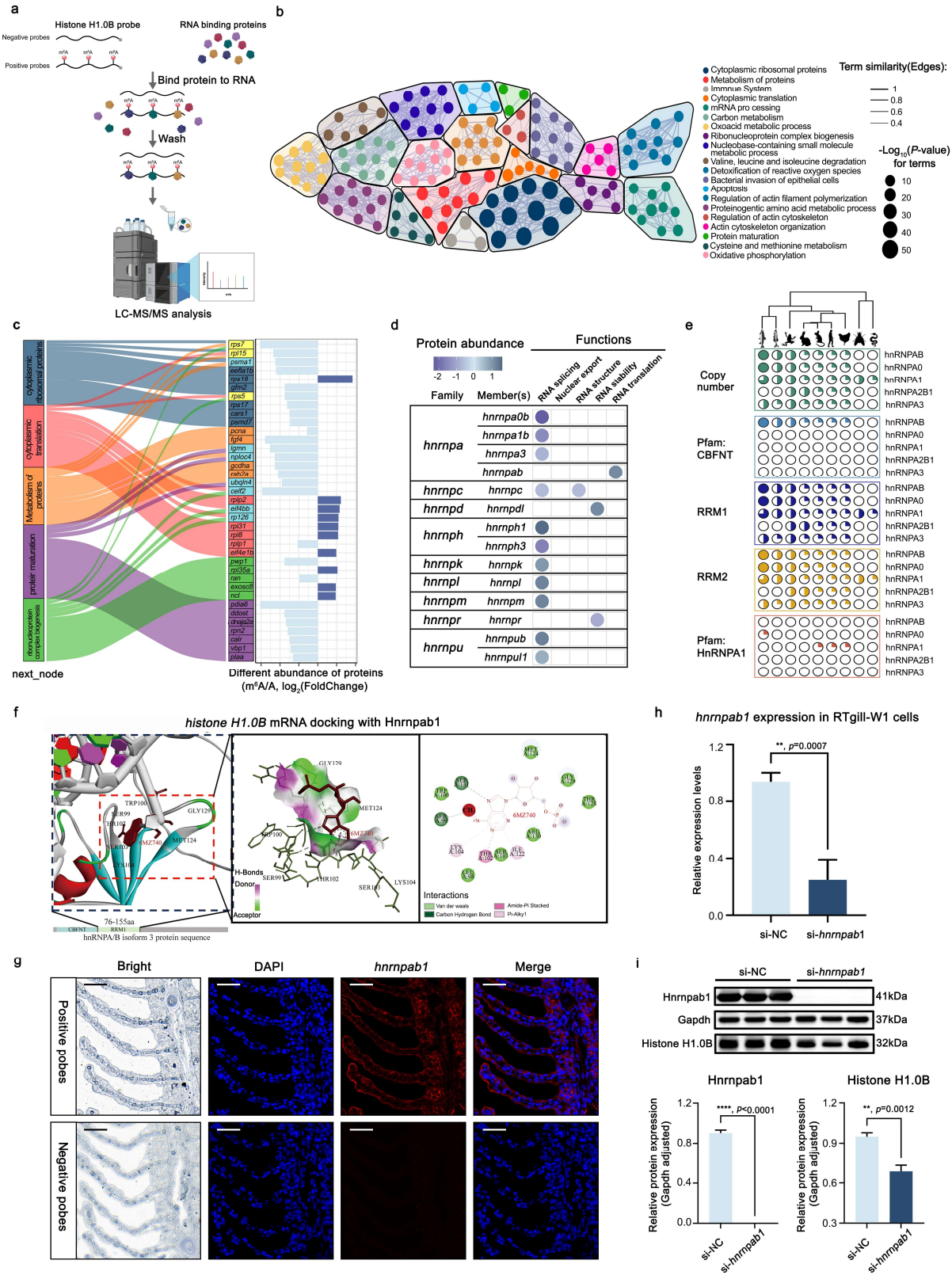


Fig. 3 Hnrnpab1 is a reader protein that enhances the translation efficiency of *histone H1.0B*.

2.4 Re-modeling chromatin accessibility activates *tonebpa1* gene when confronting to seawater

To further explore the potential chromatin regulatory roles of *histone H1.0B*[49–51], we used ATAC-seq to profile chromatin openness in *O. mykiss* gill, contrasting FW and SW smolt groups[52]. Open chromatin regions are available for transcription factor (TF) binding, with many representing active regulatory elements. Our datasets captured the expected nucleosome banding pattern, and showed strong enrichment around TSS regions (Fig. 4a-b). Leveraging our biological replicates, we identified 27,180 and 19,673 reproducible open chromatin regions in FW and SW groups, respectively (Fig. 4c; Supplementary Fig. 8a-b). Of these, 14,718 peaks were shared by both groups, whereas 12,462 and 4,955 were FW- and SW-specific, respectively (Fig. 4c). Overall, gill chromatin accessibility was strongly regulated by salinity, with the lower number of open chromatin regions in the SW group occurring in parallel to enhanced protein abundance of Histone H1.0B (Fig. 4c), suggesting a causal association.

FW-specific open chromatin regions were linked to 9,731 coding genes (Supplementary Data 6). These included master cell-cycle regulators including *cdk1*, *cdk4*, *cdc6* and *ccnb1*[49–51] and were overall enriched in cell cycle functions (Fig. 4d-e; Supplementary Fig. 8d; Supplementary Data 7). We also identified enriched TF motifs in the FW-specific open chromatin regions compared to the SW group (Fig. 4f). Of them, *abf2*, *boris* and *ap-1* TFs were predicted to bind to these FW-specific open chromatin regions near cell-cycle regulator genes

234 in gill, such as *orc3*, *ccnb1 wee1_a* as well as *wee1_b*[53–55] (Fig. 4g). However, cell-cycle
235 regulator genes linked to FW-specific open chromatin regions were downregulated in the SW
236 group (Fig. 4c & 4e). As these regions, which largely represent promoters, were not identified
237 as open chromatin in SW, our results suggest cell-cycle progression was arrested or delayed
238 after entering seawater, likely via reduced accessibility of *cis*-regulatory elements.

239 We assumed the 4,955 SW-specific open chromatin regions have roles in salinity adaptation
240 (Fig. 4c). The genes linked to these regions were most strongly enriched for the Glioma, ErbB
241 and MAPK pathways (Fig. 4h). These signaling pathways share numerous genes, and many
242 were both upregulated in SW and linked to SW-specific open chromatin regions, for instance
243 encoding kinase and signal transduction molecules PLCγ, PKC, Ras, ERK, PI3K, AKT and
244 GSK (Fig. 4i)[56–58]. These results suggest that the remodeling of chromatin after transitioning
245 to seawater led to the activation of diverse signaling pathways gill, which could support
246 osmoregulatory adaptations.

247 A common target gene of these kinases in mammals is TonEBP (Tonicity-responsive
248 enhancer-binding protein; also known as NFAT5, Nuclear factor of activated T-cells 5), which
249 is a master gene for hyperosmotic adaptation[59,60] (Fig. 4j). While humans have a single gene,
250 we identified 4 paralogues of *tonebp* in *O. mykiss* on different chromosomes (Fig. 4j;
251 Supplementary Fig. 9a-b), likely due to the history of WGD events in salmonid evolution[60,61].
252 Paralogue *tonebp* genes were found to differ substantially in their gene structures (Fig. 4j;
253 Supplementary Fig. 9b). It is *tonebpa1* in *O. mykiss* that underwent the prominent exon
254 shuffling and subsequent functional domain rearrangement, divergent with the other *tonebp*
255 paralogues in *O. mykiss* as well as homologues across other salmonids[61] (Fig. 4j;

Supplementary Fig. 9b). Meanwhile, among the 4 paralogues in *O. mykiss*, only *tonebpa1* showed up-regulation in seawater conditions, supported by both RNA-seq and qPCR (Fig. 4k; Supplementary Fig. 9c). These observations imply the lineage-specific evolutionary fate of *tonebp* genes in salmonids.

To further validate the regulatory relationships between upstream signal kinases and *tonebpa1*, inhibition of ERK and GSK3β experiment *in vitro* was conducted, providing convincing evidence for the regulation relationships between well-known kinases and *tonebpa1* (Fig. 4l-m; Supplementary Fig. 9d). Overall, these results show that *tonebpa1* plays an important role in seawater adaptation in *O. mykiss*.

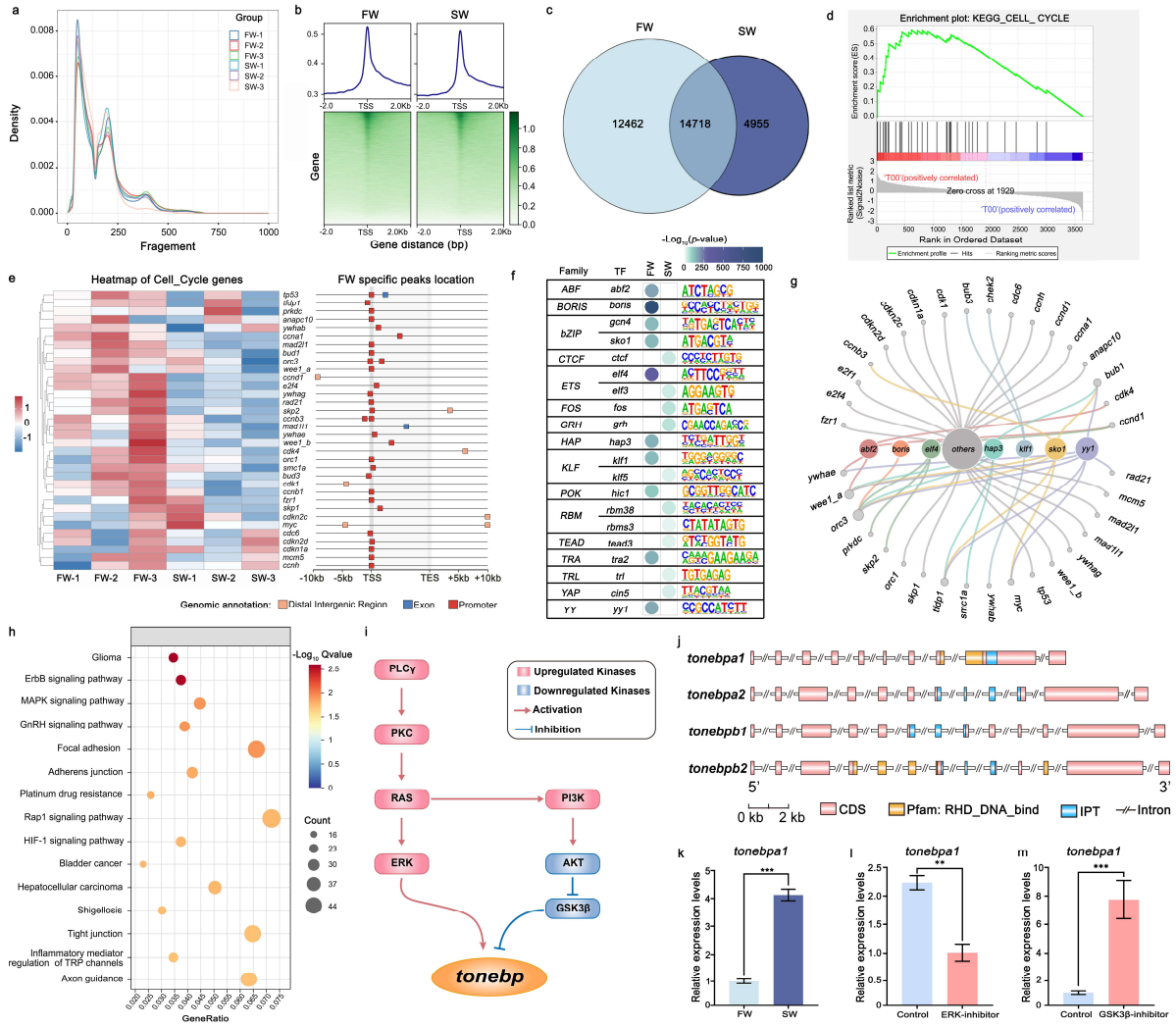


Fig. 4 Chromatin remodeling in the gill of *O. mykiss* smolts challenged with seawater.

2.5 Involvement of *tonebpa1* in ionocyte proliferation and osmotic balance for salinity adaptation

We next performed experiments to test the potential functions of *tonebpa1* in *O. mykiss* gills during salinity adaptation. Firstly, we observed that *tonebpa1* mRNA highly co-localized with *nka*, a classic marker of teleost ionocytes, a specialized cell type that principally acts to excrete excess Na^+ and Cl^- to maintain osmotic balance[62,63]. Following up this result, siRNA knockdown of *tonebpa1* was performed using RTgill-W1 cells (Fig. 5b; Supplementary Fig. 10a-b). The si-NC (control) and si-*tonebpa1* groups were incubated in normal (300 mOsm/L) and hyper-osmotic (700 mOsm/L) conditions for 24h before RNA-seq was performed (Fig. 5b). GO enrichment analysis revealed a clear association between cell cycle regulation and *tonebpa1*-dependent DEGs among the salinity conditions (Fig. 5c; Supplementary Data 8). Next, to determine potential target genes of *tonebpa1*, we scanned for its binding motif in the promoters of these DEGs (Supplementary Fig. 10c; Supplementary Data 9), revealing 70 candidates, including several cell-cycle regulators (Fig. 5d) such as *mcm2* and *purb* (DNA replication); *smc4*, *cenpl* and *cenpu* (chromosome segregation); and *ensa* and *gadd45a* (cell cycle checkpoint). Dual-luciferase reporter assays confirmed the regulatory relationship between *tonebpa1* and several of these genes (Fig. 5e).

To further explore the effects of *tonebpa1* on cell cycle, we conducted a cell proliferation experiment with RTgill-W1 cells at an osmotic gradient ranging from 300 to 1100 mOsm/L. No differences were found in cell proliferation between the si-NC and si-*tonebpa1* groups

under 300 mOsm/L (Fig. 5f-g). However, proliferation was partially impaired in the si-NC group with increased osmotic stress, while many more cells lost proliferative ability in the si-*tonebpa1* group under hyperosmotic conditions. Thus, *tonebpa1* appears necessary for the normal proliferation of *O. mykiss* gill cells under hyper-osmotic conditions. To further support this finding, flow cytometry was performed for si-NC and si-*tonebpa1* groups under 300 and 700 mOsm/L (Fig. 5h). As judged by cell-cycle phase ratios, the si-*tonebpa1* group showed a large increase of G2/M phase cells at the higher osmotic stress (Fig. 5h), which is likely to prolong and arrest the cell cycle and hence limit cell proliferation. Gluorescence-activated cell sorting (FACS) showed that the proportion of ionocytes in the si-*tonebpa1* group was strongly decreased across the tested gradient (Fig. 5i). Finally, Nka enzyme activity was observed to be highly repressed in the si-*tonebpa1* group (Fig. 5j).

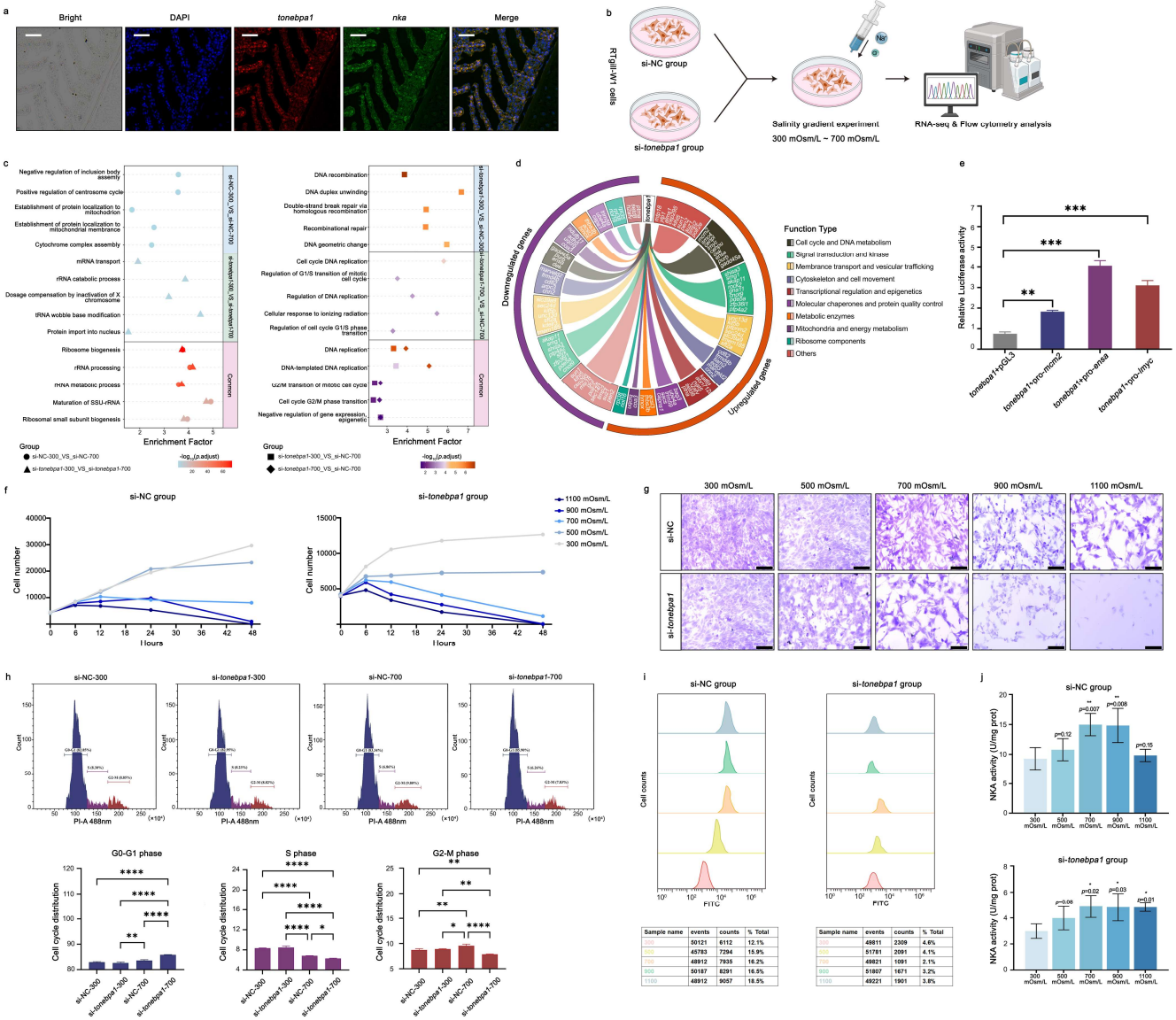


Fig. 5 *tonebpa1* regulates the ionocyte cell cycle under hyperosmotic conditions.

Therefore, *tonebpa1* is indispensable for maintaining proliferation ability and cell-cycle integrity of ionocytes in response to high-salinity and hyper-osmotic environment in the gill epithelium of *O. mykiss* smolts (Fig. 6).

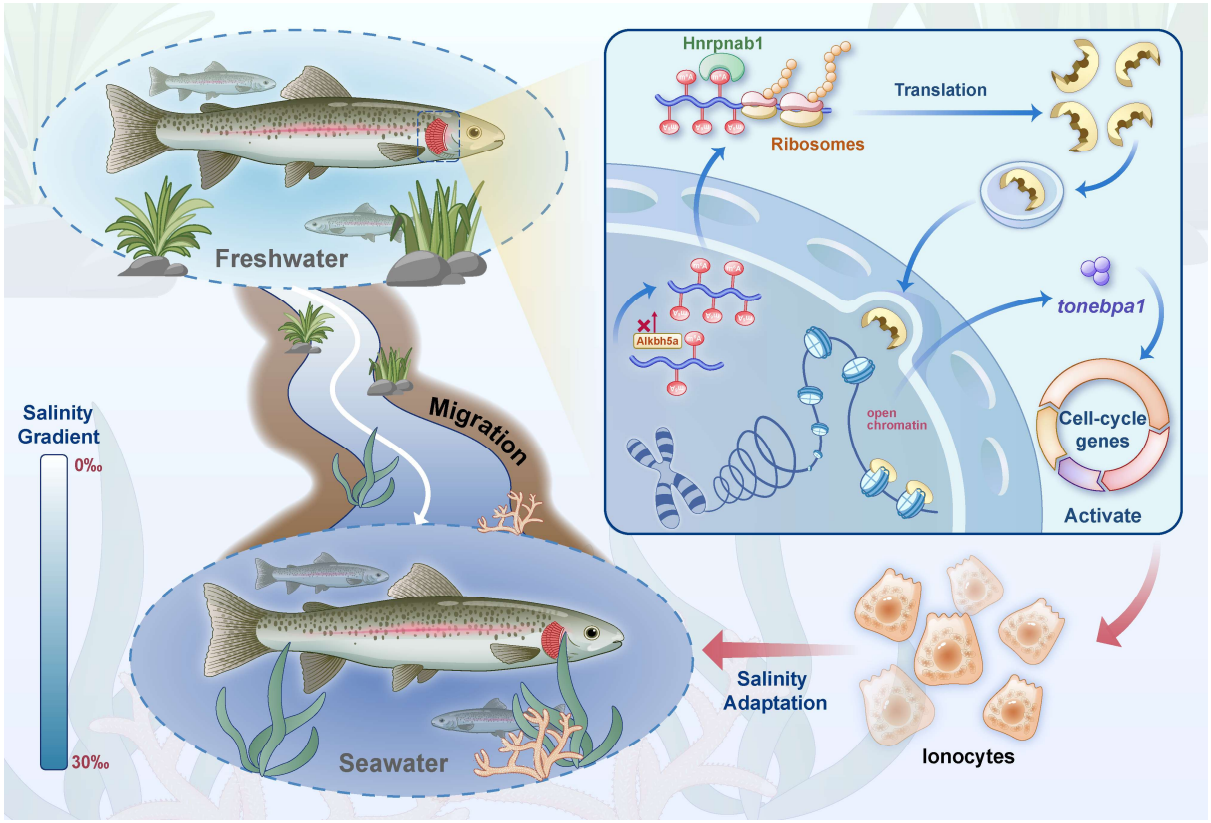


Fig 6 Proposed model for m^{6}A-dependent regulation of salinity adaptation and osmoregulation in gill epithelium of *O. mykiss* smolts.

3. Discussion

RNA m^{6}A methylation is now established to represent a crucial regulator of animal stress responses. Nonetheless, its functions remains poorly understood in fish, including with respect to the dramatic osmoregulatory stresses faced by anadromous lineages when migrating across salinity gradients[2-3]. In this work, we found that several of the master vertebrate methyltransferase and demethylase genes are retained as salmonid-specific paralogs from the Ss4R WGD event, which may have allowed them to evolve divergent roles through subfunctionalization and neofunctionalization, while some of the extra copies appear to be in the process of pseudogenization[64]. Our *in vitro* and *in vivo* results support that one *alkbh5a*

demethylase paralog was highly seawater-sensitive in *O. mykiss*, and potentially serves as the key regulator in guiding m^6A methylation. Though reports are otherwise lacking in animals, the roles of ALKBH5 homologs in salinity tolerance and osmoregulation are extensively documented in plants[65–67] Thus, we propose that *alkbh5* genes share conserved functions that help cope with osmotic stress, which date back to at least the common ancestor of plants and animals.

We went on to show that when anadromous rainbow trout are confronted with seawater, the gill cell-cycle is temporarily arrested, associated with loss of chromatin openness at master cell cycle genes that were transcriptionally downregulated, such as *cdk1*, *cdk4*, *cdc6* and *ccnb1*[49–51]. This transition may serve to protect cells from DNA damage[68], prevent DNA replication from interfering with the upregulation of adaptive genes to osmoregulation[69] or re-allocate energy for biology processes required in the hyperosmotic environment.

However, *tonebpa1* gene was the only paralog that found to be activated in seawater with function in regulating the cell cycle of gill ionocytes in *O. mykiss* smolts. This gene has key roles in the hyper-osmotic adaptation in the mammalian kidney[59,60] and was upregulated in cells under osmotic stress in both tilapia[70] and Atlantic salmon[61]. We identified 4 *tonebp* paralogs in *O. mykiss*, which were likely derived from the teleost-specific WGD followed by the Ss4R WGD. Despite sharing the duplicated *tonebp* genes in Atlantic salmon and *O. mykiss*, their gene structures exhibited obvious divergence, especially *tonebpa1* with dominant function to cope with high-salinity environment in *O. mykiss*[61]. It points to a lineage-specific evolutionary fate of *tonebp* genes in after its splitting from their ancestors with Atlantic salmon. In *O. mykiss*, *tonebpa1* becomes dominant copy responsible for maintaining ionocyte

proliferation and osmotic balance, which were jointly supported by *in vitro* and *in vivo* findings. The present study proposed a m^6A-dependent mechanism with functional significance to re-model chromatin accessibility and activate *tonebp1a*, responsible to salinity adaptation and osmoregulation in gill epithelium of *O. mykiss* smolts during seaward migration.

In summary, our findings support a novel model of salinity adaptation and hyperosmotic stress regulation in the gill of anadromous *O. mykiss* smolts during their seaward migration. When confronted with rising salinity, *alkbh5a* regulates m^6A methylation on *histone H1.0B* mRNAs to enhance their translation efficiency by recruiting the reader protein HnRNPAB. Changes in protein abundance of Histone H1.0B, a nucleosome linker protein, in turn remodels chromatin accessibility and activates signaling pathways activating *tonebpa1*, which contributes to maintaining cell-cycle integrity, particularly in ionocytes, under seawater conditions. These findings overall provide novel molecular-level insights into salinity adaptations in anadromous salmonids, highlighting the significance of RNA epigenetic modifications in teleost osmotic stress responses.

4. Materials and Methods

4.1 Ethics Statement

All experimental protocols were performed in strict accordance with the ethical guidelines and standards of the Institutional Review Board at Ocean University of China (Permit Number: OUC-AE-2022-010). Fish were killed with a schedule 1 method, using an overdose of MS-222 (Cat. no. E10521, Sigma-Aldrich; dosage: 500 mg/L) followed by destruction of the brain.

4.2 Smoltification induction and *in vivo* salinity experiment

O. mykiss eggs (Troutlodge commercial strain; Puget Sound, Washington, USA) were

362 fertilized in Nov 2020 and transferred to Qingdao (China) at the eyed stage. Then, they were
363 cultured in fresh water for 6 months with natural photoperiod. Parr-smolt transformation
364 experiments were conducted in May 2021, following previous Clark report[72]. 300 juveniles
365 (body weight: 108 ± 7.09 g, body length: 16 ± 2.85 cm) were randomly held in 3 circular
366 tanks (volume = 3.5 m^3) equipped with automated temperature and light control. An increasing
367 temperature regime (7 to 13 ℃; 1 ℃/week) was used synergistically with increasing day length
368 (12 h light: 12 h dark/d to 15 h light: 9 h dark/d; light increasing by 30 min/week with constant
369 intensity of 50 lx at the tank surface) to promote smoltification. Hand feeding was conducted
370 twice daily beginning at 08:00 and 16:00. After 6 weeks, all juveniles have completed
371 smoltification, transforming from dark-colored parr to silver colored smolts. After an
372 acclimation period, these smolts were exposed to gradually increasing salinity (6‰ per day
373 until 30‰). Three individuals per tank were randomly sampled at 0‰, 6‰, 12‰, 18‰, 24‰,
374 and 30‰ salinity. Blood was collected from the caudal vein until the gill epithelium appeared
375 light pink or nearly white. Gill epithelium was carefully excised using sterile dissecting
376 equipment, placed into RNase-free 2 mL centrifuge tubes, flash frozen in liquid nitrogen until
377 use in analyses described in sections that follow.

378 **4.3 RTgill-W1 hyperosmotic experiment**

379 The RTgill-W1 cell line, derived from *O. mykiss* gill epithelium[73], is a highly established *in*
380 *vitro* system for studying gill osmoregulation[74,75]. We purchased RTgill-W1 from American
381 Type Culture Collection (ATCC CRL-2523™, Manassas, USA), which was cultured in L-15
382 medium (Cat. no. 11415064, Thermo Fisher Scientific) supplemented with Fetal Bovine Serum
383 (Cat. no. A5669701, Thermo Fisher Scientific) and penicillin/streptomycin (Cat. no. 15140122,

Sigma-Aldrich). Cells were cultured at 19 °C. For the salinity experiment, ~ 200,000 cells with > 95% viability were selected and then incubated in the same culture medium with or without dissolved sterile sea salt added (to achieve osmolarity levels from 300-900 mOsm/L).

4.4 Quantification of total m^{6}A levels

Total RNA was extracted from gill epithelium or RTgill-W1 cells. RNA concentration estimated using a Nanodrop 2000 Spectrophotometer (Thermo Fisher Scientific). Thereafter, RNA samples were used to quantify total m^{6}A using the EpiQuik m^{6}A RNA Methylation Quantification Kit (Cat. no. P-9005-48, Enzo Life Sciences). Briefly, the m^{6}A standard solutions and equal amount of RNA (200 ng) were mixed with capture antibody, detection antibody and booster solutions. A standard curve of m^{6}A levels was colorimetrically constructed by reading the absorbance at 450 nm and used to estimate m^{6}A levels of gill epithelium and RTgill-W1 cells.

4.5 Identification of m^{6}A regulators in the *O. mykiss* genome

Homology and domain-based approaches were used to identify m^{6}A regulator genes in *O. mykiss* genome (USDA_OmykA_1.1). In homology approach, amino acid sequences of known m^{6}A regulator genes from human, mouse and zebrafish were downloaded from NCBI (Supplementary Table 1) and used as queries searches against amino acid sequences encoded by *O. mykiss* genes by BLAST+ (v2.13.0)[76] software. In domain-based method, hidden Markov model of conserved m^{6}A writer domains was searched across all amino acid sequences using HMMER (v3.3.2)[77]. Full-length amino acid sequences in representative vertebrates and *O. mykiss* were aligned using ClustalW (v2.1)[78], which were then constructed phylogenetic trees using maximum likelihood in RAxML (v8.2.12)[79] with 1,000 ultrafast bootstrap replicates.

406 **4.6 RT-qPCR and Western blot experiments**

407 Intron-spanning primers were designed and validated with standard curves to estimate
408 amplification efficiency (Supplementary Table 2). For duplicated genes, paralog-specific
409 primers were designed and checked against *O. mykiss* genome. RT-qPCR was run on the Bio-
410 Rad CFX96 Real-Time Detection System using ChamQ Universal SYBR qPCR Master Mix
411 (Cat. no. Q711-02, Vazyme). It was conducted as follows: initial denaturation at 95 °C for 30
412 s, followed by 40 cycles of 95 °C for 10 s and extension at 60 °C for 30 s. Melting-curve
413 analysis confirmed the presence of a single specific product. Relative expression levels was
414 calculated based on the $2^{-\Delta\Delta Ct}$ method and *18s rRNA* worked as reference[80].

415 For western blots, gill epithelium or RTgill-W1 cells were lysed in RIPA with protease
416 inhibitor, and centrifugated for proteins in supernatants. After quantification, 30 μg of total
417 protein was separated on SDS-PAGE and transferred onto the PVDF membranes.
418 Immunoblotting analysis was conducted with anti-Alkbh5a (rabbit, 1:5000, Cat. no. 67811-1-
419 Ig, Proteintech), anti-Mettl3a (rabbit, 1:2000, Cat. no. 2125, Cell Signaling Technology), anti-
420 Histone H1.0 B (rabbit, 1:2000, Cat. no. 18201-1-AP, Proteintech), and anti-Hnrnpab1 (rabbit,
421 1:2000, Cat. no. 31175-1-AP, Proteintech). The membranes were incubated with HRP-
422 conjugated mouse anti-rabbit secondary antibodies (1:2000, Cat. no. SA00001-2, Proteintech),
423 followed by the detection of protein signals using ChemiDoc™ Imaging System (Bio-Rad,
424 Hercules, USA) and ImageJ software.

425 **4.7 Plasmid construction and overexpression experiment**

426 Primers for CDS amplifying of *mettl3a* and *alkbh5a* were designed using SnapGene software
427 (Supplementary Table 2). Restriction enzyme recognition sites and protective bases were added

to 5' ends of primers according to restriction enzymes. Full-length *mettl3a* and *alkbh5a* were amplified using cDNA from gill epithelium using PCR (Supplementary Table 2). These products were cloned into pEGFP-N1 overexpression vector, which were separately transfected into RTgill-W1 cells using Lipofectamine 3000 (Cat. no. L3000075, Thermo Fisher Scientific). The empty cloning vector was used as negative control and transfection efficiency was examined by RT-qPCR.

4.8 MeRIP-seq analysis and MeRIP-qPCR assay

Total RNA of gill epithelium tissues from FW and SW groups incubated with Magnetic Oligo (dT) Beads to extract poly $(A)^+$ mRNA. Around 10 μg fragmented mRNA was used for library construction of input-seq samples. The remaining mRNA (~ 40 μg) was incubated with 15 μg anti-m^6A polyclonal antibody in 1 × IP buffer. Following the incubation with protein A/G agarose beads, the captured mRNA fragments were immediately eluted from beads using elution buffer. After 75% ethanol precipitation, mRNAs were prepared for library construction of IP-seq samples. Libraries (n=3 for FW and SW group) were finally sequenced on the Illumina Novaseq 6000 platform.

For MeRIP-seq analysis, low-quality sequences were trimmed using fastp v0.23.2[80] (Supplementary Table 3). Hisat2 v2.2.1 was used to align clean reads to *O. mykiss* genome [82]. Reads generated by PCR duplication were marked and fully removed in all the input- and IP-seq samples using sambamba v0.8.2[83]. Only unique mapping reads were kept for peak calling using MeTDiff R package v1.0[85] and enrichment analysis. The corresponding input-seq samples served as controls to normalize mRNA abundance. Simultaneously, MeTDiff calculated *P* values for each peak using a likelihood ratio test, with differentially methylated

450 m^{6}A peaks accepted as FDR < 0.05 and |fold change| > 1.5. All m^{6}A peaks were annotated
451 using ChIPseeker v1.34.1[86]. *De novo* motif searches against m^{6}A peaks were conducted using
452 findMotifsGenome.pl script within HOMER v4.11[87]. Enrichment analyses were performed
453 using clusterProfiler v4.6.0[88]. IGV v2.15.2[89] was used to visualize read coverage containing
454 m^{6}A peaks of interest.
455 RNA-seq datasets comparing FW and SW groups were acquired from a previous study
456 (accession: SAMN29005439). The raw reads were trimmed, then aligned to the same reference
457 genome for *O. mykiss*. A count matrix containing coding genes was constructed using
458 featureCounts package v2.0.3[90]. FPKM was calculated to normalize the expression (all non-
459 zero values taken forward for analysis). Meanwhile, DEGs between FW and SW groups were
460 calculated using DESeq2 R package v1.38.0[91], using a cut-off of $\log_2$|FoldChange| > 1 and
461 FDR < 0.05.
462 MeRIP-qPCR was performed to validate MeRIP-seq results. Six genes harboring
463 significantly altered m^{6}A peaks between the FW and SW groups were randomly selected. Site-
464 specific primers were designed according to the precise m^{6}A methylation loci (Supplementary
465 Table 2). Briefly, the fragmented mRNA, prepared as described above, was subjected to IP
466 under the same conditions as MeRIP-seq, by incubation with anti-m^{6}A antibody and capture
467 antibody-bound RNA fragments via A/G beads. After washing to remove non-specific binding,
468 the enriched m^{6}A -modified RNA (IP) was competitively eluted. Meanwhile, a portion of RNA
469 without IP was retained as input control. Both IP and input samples were purified and reverse
470 transcribed into cDNA. Site-specific primers targeting the identified m^{6}A peak regions
471 (Supplementary Table 2) were used for qRT-PCR. The m^{6}A enrichment level was calculated as

the percentage of IP relative to input, representing the methylation level at specific sites. Each experiment was performed with n=3 samples (with 3 technical replicates per sample).

4.9 ATAC-seq analysis

Gill epithelium from FW and SW groups were minced into pieces < 1 mm. Gentle centrifugation was conducted and the supernatant discarded. After that, type II collagenase (Cat. no. BS164, Biosharp) was added for incubation and filter our using 40 μm cell strainer. Cells were washed and resuspend using HBSS (Cat. no. BL559A, Biosharp), which were then submitted for cell counting and viability assessment via Trypan blue staining. A total of 5×10^4 viable cells (cell viability > 90%) from individuals of FW and SW group were used to construct library using TruePrep DNA Library Prep Kit V2 for Illumina (Cat. no. TD501, Vazyme) (n=3 each for FW and SW group). Libraries were PCR-amplified for 12 cycles. DNA was purified using VAHTS DNA Clean Beads (Cat. no. N411-01, Vazyme). Libraries were evaluated for size distribution with the Agilent 2100 Bioanalyzer system (Agilent Technologies, Santa Clara). Finally, libraries were sequenced on the Illumina NovaSeq 6000 platform.

Raw ATAC-seq reads were trimmed using fastp v0.23.2. Clean reads were aligned to the reference genome of *O. mykiss* using bwa-mem v0.7.17[93]. MACS2 v2.2.7.1[91] was used for peak calling (parameters: "-g 2335487453 -q 0.01 --nomodel --extsize 150"). Peaks were considered reproducible when identified in at least two replicates. Intervene v0.6.5[95] was used to intersect these peaks, resulting in FW- and SW-specific sets. Motif enrichment within reproducible peaks was achieved using the *de novo* mode by the findMotifsGenome.pl in HOMER.

4.10 RNA m^{6}A probe synthesis and RNA pull-down assays

Biotin-labeled ssRNA probes of *histone H1.0B* mRNA, containing m^6A (positive probe) or adenosine (negative probe), were biosynthesized by Sangon Biotechnology Services Co., Ltd. (Shanghai, China). Information on probe sequences were given in Supplementary Table 5. Thereafter, RNA pull-down was performed using the Pierce™ Magnetic RNA-Protein Pull-Down Kit (Cat. no. 20164, Thermo Fisher Scientific). Positive and negative probes were labeled with biotin and streptavidin beads, followed by incubation with protein extracted from gill from FW and SW groups. The beads were boiled to elute proteins from RNA-protein complexes. Partial eluents were resolved via SDS-PAGE for silver staining. The other eluents were subjected to LC-MS/MS analysis.

4.11 LC-MS/MS analysis

The eluents generated from RNA pull-down were submitted to LC-MS/MS to identify and quantify proteins binding to m^6A positive and negative probes. Proteins in eluents were digested into peptides. Before on-line detection using an UltiMate 3000 RSLCnano system coupled to a Q Exactive HF mass spectrometer (Thermo Fisher Scientific) in positive electrospray ionization mode with a nanospray voltage of 2.4 kV and 305 °C, peptides were loaded and separated by reverse phase UPLC on C18 column (75μm×25cm, 1.9μm particle size, 120Å pore size, Acclaim^{TM} 120, ThermoFisher). Chromatography gradients started from 94% solution A (0.1% formic acid and 3% DMSO in 80% ACN) and 6% solution B (0.1% formic acid in water) at a flow rate of 300 nL/min. Then, the gradient was set as follows: 5 min, 89% A; 20 min, 85% A; 43 min, 75% A; 62.5 min, 53% A; 63 min, 10% A; and maintained at 10% A until 65 min. The full-scan MS spectra was conducted with 350-1500m/z, and HCD was set as 24. MS files were processed by MaxQuant v2.0.3.0.[96]. Based on identified thresholds

of FDR < 0.01, andromeda worked as the search engine across the UniProtKB and NCBI public database as well as proteins encoded by genes of genome used elsewhere[97]. Meanwhile, these peptides assigned to protein groups with FDR < 0.01. Protein abundance between positive and negative probes was compared using Edge R package v3.40.2[98] using a cut-off of $\log_2|\text{Foldchange}| \geq 1$ and FDR < 0.05. Metascape was used to identified enriched interaction relationships among proteins showing different abundance, visualized using Cytoscope v3.9.1[96,97].

4.12 Molecular docking

To investigate the recognition relationships, amino acid sequences of Hnrnpab1 and nucleotide sequences of *histone H1.0B* mRNA were submitted to AlphaFold 3 server to predict RNA-protein interactions. m^6A were specifically introduced at adenosine residues 740, 772, 796, and 802 of *histone H1.0B* mRNA. The co-evolutionary signals from RNA consensus sequences and protein multiple sequence alignments jointly refined the binding interfaces. Atom-level 3D coordinates were optimized via heterogeneous GNNs. Multi-species training model was integrated with diverse complexes using adversarial domain adaptation to mitigate species-specific biases. Architecture based on the Monte Carlo dropout algorithm outputted the interface residues, conformational changes, and uncertainty quantification. Ultimately, an atomic-level accurate conformation of Hnrnpab1 protein docking to *histone H1.0B* was achieved. Discovery Studio v19.1 was employed to analyze interaction patterns.

4.13 Effects of ERK and GSK3β inhibition on *tonebpa1* expression

To confirm regulatory relationships between target kinases (ERK and GSK3β) and *tonebpa1*, RT-gill W1 cells were treated with ERK inhibitor FR180204 (Cat. no. SD5978, Beyotime) and

538 GSK3β inhibitor CHIR99021 (Cat. no. SH2242, Beyotime). FR180204 and CHIR99021 were
539 added to the culture medium, and incubated for 24 h. Total protein was extracted, and Western
540 blot was performed as described in section 4.6. The inhibitory effects of ERK and GSK3β were
541 evaluated using Phospho-ERK1/2 (Thr202/Tyr204) recombinant monoclonal antibody (rabbit,
542 1:2000, Cat. no. 80031-1-RR, Proteintech) and Phospho-GSK3β (Ser9) monoclonal antibody
543 (mouse, 1:2000, Cat. no. 67558-1-Ig, Proteintech). Meanwhile, RT-qPCR was performed for
544 detection of *tonebpa1* expression.

545 **4.14 Hnrnpab1 immunofluorescence staining assay**

546 For Hnrnpab1 protein staining, gill epithelium from FW and SW groups were fixed,
547 dehydrated, embedded, and sectioned at 5 μm thickness. Sections were blocked and incubated
548 with anti-Hnrnpab1 (Cat. no. 31175-1-AP, Proteintech). After washes by PBS, sections were
549 incubated with fluorescent dye-conjugated secondary antibody (Alexa Fluor 594) (Cat. no.
550 ab150080, Abcam). Nuclei were subsequently stained with DAPI (Cat. no. D1306, Thermo
551 Fisher Scientific) in PBS. Fluorescence images were acquired using an Andor Dragonfly
552 confocal microscope and processed with Imaris and ImageJ software.

553 **4.15 Dual-fluorescence *in situ* hybridization assay**

554 Gill epithelium was sectioned into 5 μm thick slides using methods described in section 4.14.
555 Probes of *tonebpa1* and *nka* (Supplementary Table 8) containing T7 or SP6 promoters were
556 amplified. Slides were hybridized with the digoxigenin-labeled *tonebpa1* probe and biotin-
557 labeled *nka* probe in a humidified chamber with gentle shaking. Subsequently, slides were
558 blocked and incubated with HRP-conjugated anti-DIG/BIO antibody (Cat. no. 11585614910,
559 Roche). Nuclei were counterstained with DAPI. Dual-fluorescence images were captured using

560 an inverted epifluorescence microscope (FV3000, Olympus) equipped with DAPI and
561 FITC/Cy3 Red filters and a Photometrics CCD camera (Photometrics, Tucson, USA). Digital
562 images were processed using ImageJ software.

563 **4.16 RNA interference, salinity experiment and RNA-seq analysis**

564 The siRNA was designed for *tonebpa1* and synthesized by Sangon Biotech (Sangon,
565 Shanghai, China) (Supplementary Table 9). The si-NC (control) was designed using the
566 BLOCK-iT^{TM} RNAi Designer tool (Supplementary Table 9). Transfection of si-*tonebpa1* (60
567 nM) and si-NC (60 nM) was performed in RTgill-W1 cells under 300-1100 mOsm/L conditions
568 using Lipofectamine 3000 (Thermo Fisher Scientific). After incubation, the transfection
569 efficiency was examined by RT-qPCR. Then, the si-NC and si-*tonebpa1* groups were used in
570 salinity experiment, followed methods described in Section 4.3. For RNA-seq, total RNA was
571 extracted from si-NC and si-*tonebpa1* groups under 300 and 700 mOsm/L conditions. High-
572 quality RNA was subjected for RNA-seq library construction followed by sequencing on an
573 Illumina Novaseq 6000 platform (n=3). Samples were named as following: si-NC-300, si-
574 *tonebpa1*-300, si-NC-700 and si-*tonebpa1*-700 groups. Analysis following the workflow
575 descripted in section 4.8.

576 **4.17 Dual-LUC assay**

577 To validate the role of *tonebpa1* in transcriptional regulation, *mcm2*, *ensa*, and *lmyc* were
578 selected from our list of candidate *tonebpa1* target genes. The promoter regions of each were
579 amplified (Supplementary Table 10) and cloned into pGL3-Basic vector using SacI (Cat. no.
580 1078S) and XhoI (Cat. no. 1094S) restriction sites (Takara Biotechnology), generating reporter
581 constructs. The *tonebpa1* coding sequence was amplified and inserted into pcDNA3.1

582 expression vector via EcoRI (Cat. no. 1040S) and KpnI (Cat. no. 1068S) sites (Takara
583 Biotechnology), serving as the effector plasmid. Transfection of HEK-293T and the dual-
584 luciferase reporter assay followed Li et al[98].

585 **4.18 Cell proliferation assay**

586 Cell proliferation was assessed using Cell Counting Kit-8 (CCK-8; Cat. no. C0038,
587 Beyotime). Briefly, RTgill-W1 cells were transfected with si-NC or si-*tonebpa1*. At 6, 12, 24,
588 and 48 h post-transfection, 10 μL of CCK-8 reagent was added to each well and incubated. The
589 absorbance at 450 nm (OD450) was measured using a microplate reader, and cell proliferation
590 was quantified based on the OD450 values.

591 **4.19 Flow Cytometry Analysis**

592 Cell viability, cell proliferation and cell cycle analyses were performed to explore the
593 potential roles of *tonebpa1* in cell process. For cell viability, RTgill-W1 cells were stained with
594 the LIVE/DEAD™ Fixable Dead Cell Stain (Cat. no. L23105, Thermo Fisher Scientific). After
595 incubation, cells were fixed with 37% formaldehyde for 15 min, washed with PBS containing
596 1% BSA, and analyzed using a FACSVerse™ flow cytometer (BD Biosciences, San Jose, CA,
597 USA; excitation 488 nm).

598 Cell cycle profiles were determined as described elsewhere[102], with minor modifications.
599 RTgill-W1 cells were treated for 24 h, fixed in 70% ethanol, and stained with PI solution (Cat.
600 no. P4170, Sigma-Aldrich) containing RNase A. DNA content was measured using a
601 FACSVerse™ flow cytometer (BD Biosciences, San Jose, CA, USA).

602 Cell proliferation was measured using the Click-iT™ EdU Flow Cytometry Assay Kit (Cat.
603 no. C10419, Thermo Fisher Scientific). RTgill-W1 cells were seeded and incubated. EdU

solution (20 μM) was added to achieve a final concentration of 10 μM, and the cells were incubated for 2 h at 37 °C. Following incubation, cells were fixed, permeabilized, and subjected to the Click reaction. Fluorescence signals were collected using a flow cytometer (BD Biosciences) at excitation/emission wavelengths of 555/565 nm.

Data availability

All data are available in the main text or the supplementary materials. The raw sequencing data of MeRIP-seq, ATAC-seq, and RNA-seq generated in this study have been deposited in the NCBI SRA database (accession numbers SAMN29005439-SAMN29005456). The processed results of MeRIP-seq, ATAC-seq and RNA-seq are available in Supplementary Data 10-14. Plasmids and cells generated in this study are available upon request.

Code availability

No custom code or software was developed for this study. Sequencing data were processed using publicly available softwares and packages as described in the Methods section, including fastp, HISAT2, SAMtools, sambamba, MeTDiff, ChIPseeker, HOMER, clusterProfiler, BWA-MEM, MACS2, Intervene, MaxQuant, edgeR, Metascape, Cytoscape and IGV. Additional scripts used for data processing and figure generation are available from the corresponding author upon reasonable request.

References:

1. Larsen, P. F. *et al.* Interpopulation differences in expression of candidate genes for salinity tolerance in winter migrating anadromous brown trout (Salmo trutta L.). *BMC Genet* **9**, 12 (2008).

2. Dodson, J. J., Aubin-Horth, N., Thériault, V. & Páez, D. J. The evolutionary ecology of alternative migratory tactics in salmonid fishes. *Biol Rev Camb Philos Soc* **88**, 602–625 (2013).

3. Klemetsen, A. *et al.* Atlantic salmon Salmo salar L., brown trout Salmo trutta L. and Arctic charr Salvelinus alpinus (L.): a review of aspects of their life histories. *Ecology of Freshwater Fish* **12**, 1–59 (2003).

4. Haugen, T. O. & Vøllestad, L. A. A century of life-history evolution in grayling. *Genetica* **112**, 475–491 (2001).

5. Zhivotovsky, L. A. Genetic history of salmonid fishes of the genus Oncorhynchus. *Russ J Genet* **51**, 491–505 (2015).

6. Keeley, E. R., Kershner, J. L., Williams, J. E. & Gresswell, R. E. Origins, Species Diversity, and Ecological Diversification in Trout and Char. *Trout and char of the world* 15–39 (2019).

7. Hoar, W. S. 4 The Physiology of Smolting Salmonids. in *Fish Physiology* vol. 11 275–343 (Academic Press, 1988).

8. Stefansson, S. O., Björnsson, B. T., Ebbesson, L. O. & McCormick, S. D. Smoltification. in *Fish Larval Physiology* (CRC Press, 2008).

9. Nichols, K. M., Edo, A. F., Wheeler, P. A. & Thorgaard, G. H. The genetic basis of smoltification-related traits in Oncorhynchus mykiss. *Genetics* **179**, 1559–1575 (2008).

10. Rousseau, K., Martin, P., Boeuf, G. & Dufour, S. Salmonid Smoltification | 6 | Metamorphosis in Fish | Karine Rousseau,. in *Metamorphosis in Fish* 167–215 (CRC Press, Boca Raton, 2012).

11. Bokar, J. A., Rath-Shambaugh, M. E., Ludwiczak, R., Narayan, P. & Rottman, F. Characterization and partial purification of mRNA N6-adenosine methyltransferase from HeLa cell nuclei. Internal mRNA methylation requires a multisubunit complex. *J Biol Chem* **269**, 17697–17704 (1994).

12. Bokar, J. A., Shambaugh, M. E., Polayes, D., Matera, A. G. & Rottman, F. M. Purification and cDNA cloning of the AdoMet-binding subunit of the human mRNA (N6-adenosine)-methyltransferase. *RNA* **3**, 1233–1247 (1997).

13. Jia, G. *et al.* N6-Methyladenosine in nuclear RNA is a major substrate of the obesity-associated FTO. *Nat Chem Biol* **7**, 885–887 (2011).

14. Zheng, G. *et al.* ALKBH5 is a mammalian RNA demethylase that impacts RNA metabolism and mouse fertility. *Mol Cell* **49**, 18–29 (2013).

15. Yang, Y., Hsu, P. J., Chen, Y.-S. & Yang, Y.-G. Dynamic transcriptomic m6A decoration: writers, erasers, readers and functions in RNA metabolism. *Cell Res* **28**, 616–624 (2018).

16. Patil, D. P., Pickering, B. F. & Jaffrey, S. R. Reading m6A in the Transcriptome: m6A-Binding Proteins. *Trends Cell Biol* **28**, 113–127 (2018).

17. Jiang, X. *et al.* The role of m6A modification in the biological functions and diseases. *Sig Transduct Target Ther* **6**, 74 (2021).

18. Ma, N. *et al.* Regulation of m6A RNA reader protein OsECT3 activity by lysine acetylation in the cold stress response in rice. *Nature Plants* **11**, 1165–1180 (2025).

19. Zhang, S. *et al.* The m6A methylation and expression profiles of mouse neural stem cells after hypoxia/reoxygenation. *Stem Cell Res Ther* **15**, 43 (2024).

20. Lu, Z. *et al.* m6A mRNA methylation analysis provides novel insights into heat stress responses in the liver tissue of sheep. *Genomics* **113**, 484–492 (2021).

21. Qi, Y., Zhang, Y., Zhang, J., Wang, J. & Li, Q. The alteration of N6-methyladenosine (m6A) modification at the transcriptome-wide level in response of heat stress in bovine mammary epithelial cells. *BMC Genomics* **23**, 829 (2022).

22. Han, D. *et al.* Anti-tumour immunity controlled through mRNA m6A methylation and YTHDF1 in dendritic cells. *Nature* **566**, 270–274 (2019).

23. Winkler, R. *et al.* m6A modification controls the innate immune response to infection by targeting type I interferons. *Nat Immunol* **20**, 173–182 (2019).

24. Ganguly, D. R. *et al.* mRNA ADENOSINE METHYLASE promotes drought tolerance through N6-methyladenosine-dependent and independent impacts on mRNA regulation in Arabidopsis. *New Phytol* **245**, 183–199 (2025).

25. Nguyen, T. K. H., Amara, U. & Kang, H. ECT8, an mRNA m6A reader, enhances salt stress tolerance by modulating mRNA stability in Arabidopsis. *Physiol Plant* **177**, e70135 (2025).

26. Zheng, H. *et al.* An mRNA methylase and demethylase regulate sorghum salt tolerance by mediating N6-methyladenosine modification. *Plant Physiol* **196**, 3048–3070 (2024).

27. Zydlewski, J. & Wilkie, M. P. Freshwater to Seawater Transitions in Migratory Fishes. in

685 *Fish Physiology* vol. 32 253–326 (Academic Press, 2013).

686 28. FAO. *Fishery and Aquaculture Statistics – Yearbook 2023*. (FAO, Rome, Italy, 2025).
687 doi:10.4060/cd6788en.

688 29. Macqueen, D. J. & Johnston, I. A. A well-constrained estimate for the timing of the
689 salmonid whole genome duplication reveals major decoupling from species diversification.
690 *Proc Biol Sci* **281**, 20132881 (2014).

691 30. Gundappa, M. K. *et al.* Genome-Wide Reconstruction of Rediploidization Following
692 Autopolyploidization across One Hundred Million Years of Salmonid Evolution. *Mol Biol Evol*
693 **39**, msab310 (2022).

694 31. Schwartz, S. *et al.* High-resolution mapping reveals a conserved, widespread, dynamic
695 mRNA methylation program in yeast meiosis. *Cell* **155**, 1409–1421 (2013).

696 32. Zhou, J. *et al.* Dynamic m(6)A mRNA methylation directs translational control of heat
697 shock response. *Nature* **526**, 591–594 (2015).

698 33. Garcia-Campos, M. A. *et al.* Deciphering the "m6A Code" via Antibody-Independent
699 Quantitative Profiling. *Cell* **178**, 731-747.e16 (2019).

700 34. Wang, X. *et al.* N(6)-methyladenosine Modulates Messenger RNA Translation Efficiency.
701 *Cell* **161**, 1388–1399 (2015).

702 35. Bednar, J. *et al.* Nucleosomes, linker DNA, and linker histone form a unique structural
703 motif that directs the higher-order folding and compaction of chromatin. *Proc Natl Acad Sci U*
704 *S A* **95**, 14173–14178 (1998).

705 36. Misteli, T., Gunjan, A., Hock, R., Bustin, M. & Brown, D. T. Dynamic binding of histone
706 H1 to chromatin in living cells. *Nature* **408**, 877–881 (2000).

707 37. Zhou, Y. *et al.* Metascape provides a biologist-oriented resource for the analysis of
708 systems-level datasets. *Nat Commun* **10**, 1523 (2019).

709 38. Meyer, K. D. *et al.* 5' UTR m(6)A Promotes Cap-Independent Translation. *Cell* **163**, 999–
710 1010 (2015).

711 39. Zaccara, S., Ries, R. J. & Jaffrey, S. R. Reading, writing and erasing mRNA methylation.
712 *Nat Rev Mol Cell Biol* **20**, 608–624 (2019).

713 40. Zhu, Z.-M., Huo, F.-C., Zhang, J., Shan, H.-J. & Pei, D.-S. Crosstalk between m6A
714 modification and alternative splicing during cancer progression. *Clin Transl Med* **13**, e1460
715 (2023).

716 41. Jin, T. *et al.* HnRNPA2B1 ISGylation Regulates m6A-Tagged mRNA Selective Export via

717 ALYREF/NXF1 Complex to Foster Breast Cancer Development. *Adv Sci (Weinh)* **11**,
718 e2307639 (2024).

719 42. Reichel, M., Köster, T. & Staiger, D. Marking RNA: m6A writers, readers, and functions
720 in Arabidopsis. *J Mol Cell Biol* **11**, 899–910 (2019).

721 43. Hu, T. *et al.* HNRNPA2B1 and HNRNPR stabilize ASCL1 in an m6A-dependent manner
722 to promote neuroblastoma progression. *Biochim Biophys Acta Mol Basis Dis* **1870**, 167050
723 (2024).

724 44. Alarcón, C. R. *et al.* HNRNPA2B1 Is a Mediator of m(6)A-Dependent Nuclear RNA
725 Processing Events. *Cell* **162**, 1299–1308 (2015).

726 45. Kwon, J., Jo, Y.-J., Namgoong, S. & Kim, N.-H. Functional roles of hnRNPA2/B1
727 regulated by METTL3 in mammalian embryonic development. *Sci Rep* **9**, 8640 (2019).

728 46. Li, B. *et al.* Regulation of HNRNP family by post-translational modifications in cancer.
729 *Cell Death Discov* **10**, 427 (2024).

730 47. Piñol-Roma, S. & Dreyfuss, G. hnRNP proteins: localization and transport between the
731 nucleus and the cytoplasm. *Trends Cell Biol* **3**, 151–155 (1993).

732 48. He, Y. & Smith, R. Nuclear functions of heterogeneous nuclear ribonucleoproteins A/B.
733 *Cell Mol Life Sci* **66**, 1239–1256 (2009).

734 49. Happel, N. & Doenecke, D. Histone H1 and its isoforms: contribution to chromatin
735 structure and function. *Gene* **431**, 1–12 (2009).

736 50. Hannon, R., Bateman, E., Allan, J., Harborne, N. & Gould, H. Control of RNA polymerase
737 binding to chromatin by variations in linker histone composition. *Journal of Molecular Biology*
738 **180**, 131–149 (1984).

739 51. Chen, Y. *et al.* Chromatin accessibility: biological functions, molecular mechanisms and
740 therapeutic application. *Sig Transduct Target Ther* **9**, 340 (2024).

741 52. Mansisidor, A. R. & Risca, V. I. Chromatin accessibility: methods, mechanisms, and
742 biological insights. *Nucleus* **13**, 236–276 (2022).

743 53. Zeng, K. *et al.* Inhibition of CDK1 Overcomes Oxaliplatin Resistance by Regulating
744 ACSL4-mediated Ferroptosis in Colorectal Cancer. *Adv Sci (Weinh)* **10**, e2301088 (2023).

745 54. Palmer, C. L. *et al.* CDK4 selective inhibition improves preclinical anti-tumor efficacy and
746 safety. *Cancer Cell* **43**, 464-481.e14 (2025).

747 55. Sun, Y. *et al.* Identification and functional characterization of IGFBP genes in Leopard
748 Coral Grouper (*Plectropomus leopardus*): Insights into growth regulation and stress response.

749 *Water Biology and Security* **4**, 100338 (2025).

750 56. Xu, J. *et al.* Activation of PLCγ/AKT/IκBα/p65 signaling increases inflammation in mast
751 cells to promote growth of cutaneous neurofibroma. *Life Sciences* **239**, 117079 (2019).

752 57. Yu, Z.-Y. *et al.* Natural Product Vibsanin A Induces Differentiation of Myeloid Leukemia
753 Cells through PKC Activation. *Cancer Res* **76**, 2698–2709 (2016).

754 58. Zhou, X., Wang, H., Burg, M. B. & Ferraris, J. D. Inhibitory phosphorylation of GSK-3β
755 by AKT, PKA, and PI3K contributes to high NaCl-induced activation of the transcription factor
756 NFAT5 (TonEBP/OREBP). *Am J Physiol Renal Physiol* **304**, F908-917 (2013).

757 59. Cheung, C. Y. & Ko, B. C. NFAT5 in cellular adaptation to hypertonic stress - regulations
758 and functional significance. *J Mol Signal* **8**, 5 (2013).

759 60. Lien, S. *et al.* The Atlantic salmon genome provides insights into rediploidization. *Nature*
760 **533**, 200–205 (2016).

761 61. Lorgen, M., Jorgensen, E. H., Jordan, W. C., Martin, S. A. M. & Hazlerigg, D. G. NFAT5
762 genes are part of the osmotic regulatory system in Atlantic salmon (Salmo salar). *Mar*
763 *Genomics* **31**, 25–31 (2017).

764 62. Hiroi, J. & McCormick, S. D. New insights into gill ionocyte and ion transporter function
765 in euryhaline and diadromous fish. *Respir Physiol Neurobiol* **184**, 257–268 (2012).

766 63. Plasschaert, L. W. *et al.* A single-cell atlas of the airway epithelium reveals the CFTR-rich
767 pulmonary ionocyte. *Nature* **560**, 377–381 (2018).

768 64. Berthelot, C. *et al.* The rainbow trout genome provides novel insights into evolution after
769 whole-genome duplication in vertebrates. *Nat Commun* **5**, 3657 (2014).

770 65. Amara, U., Shoaib, Y. & Kang, H. ALKBH9C, a potential RNA m6 A demethylase,
771 regulates the response of Arabidopsis to abiotic stresses and abscisic acid. *Plant Cell Environ*
772 **45**, 3566–3581 (2022).

773 66. Shen, H. *et al.* The AlkB Homolog SlALKBH10B Negatively Affects Drought and Salt
774 Tolerance in Solanum lycopersicum. *Int J Mol Sci* **25**, 173 (2023).

775 67. Zhao, Y. *et al.* Genome-wide identification of the AlkB homologs gene family,
776 PagALKBH9B and PagALKBH10B regulated salt stress response in Populus. *Front Plant Sci*
777 **13**, 994154 (2022).

778 68. Dmitrieva, N. I., Michea, L. F., Rocha, G. M. & Burg, M. B. Cell cycle delay and apoptosis
779 in response to osmotic stress. *Comp Biochem Physiol A Mol Integr Physiol* **130**, 411–420
780 (2001).

781 69. Saito, H. & Posas, F. Response to hyperosmotic stress. *Genetics* **192**, 289–318 (2012).

782 70. Hamar, J., Cnaani, A. & Kültz, D. Transcriptional upregulation of the myo-inositol
783 biosynthesis pathway is enhanced by NFAT5 in hyperosmotically stressed tilapia cells. *Am J*
784 *Physiol Cell Physiol* **327**, C545–C556 (2024).

785 71. Clarke, W., Shelbourn, J. & Brett, J. Growth and adaptation to sea water in 'underyearling'
786 sockeye (Oncorhynchus nerka) and coho (O. kisutch) salmon subjected to regimes of constant
787 or changing temperature and day length. *Canadian Journal of Zoology* **56**, 2413–2421 (2011).

788 72. N. C., B. *et al.* Development of a cell line from primary cultures of rainbow trout,
789 Oncorhynchus mykiss (Walbaum), gills | Request PDF. *ResearchGate* **17**, 601–611 (1994).

790 73. Lee, L. E. J., Dayeh, V. R., Schirmer, K. & Bols, N. C. Applications and potential uses of
791 fish gill cell lines: examples with RTgill-W1. *In Vitro Cell Dev Biol Anim* **45**, 127–134 (2009).

792 74. Trubitt, R. T. *et al.* Transepithelial resistance and claudin expression in trout RTgill-W1
793 cell line: effects of osmoregulatory hormones. *Comp Biochem Physiol A Mol Integr Physiol*
794 **182**, 45–52 (2015).

795 75. Camacho, C. *et al.* BLAST+: architecture and applications. *BMC Bioinformatics* **10**, 421
796 (2009).

797 76. Eddy, S. R. Accelerated Profile HMM Searches. *PLoS Comput Biol* **7**, e1002195 (2011).

798 77. Larkin, M. A. *et al.* Clustal W and Clustal X version 2.0. *Bioinformatics* **23**, 2947–2948
799 (2007).

800 78. Stamatakis, A. RAxML version 8: a tool for phylogenetic analysis and post-analysis of
801 large phylogenies. *Bioinformatics* **30**, 1312–1313 (2014).

802 79. Liu, S. *et al.* RNA-seq analysis of early hepatic response to handling and confinement
803 stress in rainbow trout. *PLoS One* **9**, e88492 (2014).

804 80. Chen, S., Zhou, Y., Chen, Y. & Gu, J. fastp: an ultra-fast all-in-one FASTQ preprocessor.
805 *Bioinformatics* **34**, i884–i890 (2018).

806 81. Kim, D., Paggi, J. M., Park, C., Bennett, C. & Salzberg, S. L. Graph-based genome
807 alignment and genotyping with HISAT2 and HISAT-genotype. *Nat Biotechnol* **37**, 907–915
808 (2019).

809 82. Tarasov, A., Vilella, A. J., Cuppen, E., Nijman, I. J. & Prins, P. Sambamba: fast processing
810 of NGS alignment formats. *Bioinformatics* **31**, 2032–2034 (2015).

811 83. Cui, X. *et al.* MeTDiff: A Novel Differential RNA Methylation Analysis for MeRIP-Seq
812 Data. *IEEE/ACM Trans Comput Biol Bioinform* **15**, 526–534 (2018).

84. Yu, G., Wang, L.-G. & He, Q.-Y. ChIPseeker: an R/Bioconductor package for ChIP peak annotation, comparison and visualization. *Bioinformatics* **31**, 2382–2383 (2015).

85. Heinz, S. *et al.* Simple Combinations of Lineage-Determining Transcription Factors Prime cis-Regulatory Elements Required for Macrophage and B Cell Identities. *Molecular Cell* **38**, 576–589 (2010).

86. Yu, G., Wang, L.-G., Han, Y. & He, Q.-Y. clusterProfiler: an R package for comparing biological themes among gene clusters. *OMICS* **16**, 284–287 (2012).

87. Robinson, J. T. *et al.* Integrative genomics viewer. *Nat Biotechnol* **29**, 24–26 (2011).

88. Liao, Y., Smyth, G. K. & Shi, W. featureCounts: an efficient general purpose program for assigning sequence reads to genomic features. *Bioinformatics* **30**, 923–930 (2014).

89. Love, M. I., Huber, W. & Anders, S. Moderated estimation of fold change and dispersion for RNA-seq data with DESeq2. *Genome Biol* **15**, 550 (2014).

90. Li, H. Aligning sequence reads, clone sequences and assembly contigs with BWA-MEM. *arXiv.org* https://arxiv.org/abs/1303.3997v2 (2013).

91. Zhang, Y. *et al.* Model-based analysis of ChIP-Seq (MACS). *Genome Biol* **9**, R137 (2008).

92. Khan, A. & Mathelier, A. Intervene: a tool for intersection and visualization of multiple gene or genomic region sets. *BMC Bioinformatics* **18**, 287 (2017).

93. Cox, J. & Mann, M. MaxQuant enables high peptide identification rates, individualized p.p.b.-range mass accuracies and proteome-wide protein quantification. *Nat Biotechnol* **26**, 1367–1372 (2008).

94. Cox, J. *et al.* Andromeda: a peptide search engine integrated into the MaxQuant environment. *J Proteome Res* **10**, 1794–1805 (2011).

95. Robinson, M. D., McCarthy, D. J. & Smyth, G. K. edgeR: a Bioconductor package for differential expression analysis of digital gene expression data. *Bioinformatics* **26**, 139–140 (2010).

96. Zhou, Y. *et al.* Metascape provides a biologist-oriented resource for the analysis of systems-level datasets. *Nat Commun* **10**, 1523 (2019).

97. Shannon, P. *et al.* Cytoscape: a software environment for integrated models of biomolecular interaction networks. *Genome Res* **13**, 2498–2504 (2003).

98. Li, W. *et al.* Regulation of jasmonic acid signalling in tomato cold stress response: Insights into the MYB15-LOXD and MYB15-MYC2-LOXD regulatory modules. *Plant Biotechnology Journal* **23**, 4246–4260 (2025).

845 99. Rieger, A. M. Flow Cytometry and Cell Cycle Analysis: An Overview. *Methods in*
846 *Molecular Biology* **2579**, 47–57 (2022).

Acknowledgements

This work was supported by grants from the China National Postdoctoral Program for Innovative Talents (BX20240343), the Taishan Industrial Program (tsls20241102), the National Natural Science Foundation of China (32202896; 32373104), the Shandong Provincial Natural Science Foundation (ZR2022QC086), the Key R&D Project of China (2024YFD2400901; 2024YFD2400300), Young Talent of Lifting engineering for Science and Technology in Shandong, China (SDAST2025QTA031) and the Marine Science and Technology Innovation Demonstration Project of Qingdao (23-1-3-hysf-2-hy). MKG was supported by Sector Plan Biology funds from the Dutch Ministry of Education, Wageningen University (No grant number). DJM was supported by BBSRC Institute Strategic Programme funding to the Roslin Institute (grant numbers: BBS/E/RL/230001A; BBS/E/RL/230001B; BBS/E/RL/230001C).

Author contributions

H. Yu and Y. Sun contributed equally to this work. H. Yu and Y. Sun conceived and designed the study, performed the experiments, analyzed the data, and drafted the manuscript; M. K. Gundappa contributed to the bioinformatic analysis. Wang participated in sample collection and experimental work; J. He, Y. Lu and C. Xin assisted with experiments and data collection; D. Li, Y. Qu and H. Zhu contributed to data analysis; D. J. Macqueen contributed to the design of experiments and analyses, and reviewed and edited the manuscript draft; Q. Gao supervised the study and revised the manuscript; Y. Tian conceived the project, supervised the study, and finalized the manuscript. All authors provided intellectual input and approved the final version of the manuscript.

869

870 **Competing interests**

871 The authors declare no competing interests.

Figure legends

Fig. 1 Alkbh5a is a major regulator of m^{6}A methylation in the gill of *O. mykiss* smolts during salinity adaptation. (a) Schematic of experimental design, where smolts were challenged with different salinities to mirror the natural migration of anadromous salmonids from freshwater (FW) into seawater (SW). (b) Ratios of m^{6}A/A in total poly(A)-tailed RNA in gills of smolts under FW and SW; (c) Species phylogeny depicting the retention of orthologs for methyltransferase (writer) and demethylase (eraser) family member genes in representative vertebrates and *O. mykiss*, according to maximum likelihood phylogenetic analyses (Supplementary Fig 2); (d-e) Expression of *mettl3a* and *alkbh5a* genes in gill tissue of smolts under gradient salinity conditions, ranging from 0‰ (FW) to 30‰ (SW); (f-g) Validation of *mettl3a* and *alkbh5a* gene expression responses in RTgill-W1 cells between 300 mOsm/L and 900 mOsm/L. Relative expression levels of *mettl3a* and *alkbh5a* genes in were determined by RT-qPCR; (h-i) Western blotting showing the abundance of Mettl3a and Alkbh5a proteins in gill tissues of smolts under FW and SW; (j-k) Ratios of m^{6}A/A in poly(A)-tailed RNA in overexpressed *mettl3a* and *alkbh5a* genes in RTgill-W1 cells. Differences were considered as significant using t-tests (*p<0.05, **p<0.01, ***p<0.001).

Fig. 2 Transcriptome-wide signatures of m^{6}A methylation and identification of *histone H1.0B* as an important substrate of Alkbh5a. (a) Circos visualization of smolt gill m6A methylation signatures and chromatin accessibility patterns across the O. mykiss genome, including Ss4R-retained collinear blocks, chromosomes, GC content, coding gene density, DEGs between FW and SW groups, m^{6}A peaks, differential m^{6}A peaks, total chromatin regions, and FW- or SW-specific open chromatin regions. Data were calculated in 3 Mbp bins; (b) Differential abundance of m^{6}A methylation between FW and SW groups, with hypo- and hyper methylated m^{6}A peaks shown with brown points. Red and green points show differential m^{6}A peaks located in upregulated and

894 downregulated DEGs, respectively, with point sizes corresponding to fold-change differences in expression. (c)
895 Enriched motifs in all m^{6}A peaks and differential m^{6}A peaks; (d) Genomic distribution of all m^{6}A peaks and
896 differential m^{6}A peaks; (e) Enriched GO terms among genes within the hypo- and hyper-methylated m^{6}A peaks.
897 Accumulation of differential methylation abundance (log_2|FoldChange|) in enriched genes is show using density
898 plots, where gene counts in enriched terms correspond to point sizes; (f) Genomic tracks showing comparisons of
899 m^{6}A methylation profiles in *histone H1.0B* (gene model at top, exon regions in dark blue) between FW and SW
900 groups. Cyan and navy colors show respective signals from IP-seq samples (n=3) in FW and SW groups (yellow
901 and red tracks show signals for the matching input-seq samples). The gray bar shows the hyper-methylated peak
902 in *histone H1*; (g) Schematic model for how Histone H1.0B acts as a nucleosome linker. (h) MeRIP-qPCR
903 comparing the relative abundance of m^{6}A methylation for *histone H1.0B* mRNA in FW and SW groups; (i)
904 MeRIP-qPCR comparing the relative abundance of m^{6}A methylation in *histone H1.0B* in RTgill-W1 cells
905 following overexpression of *alkbh5a*; (j) RT-qPCR comparing *histone H1.0B* expression in FW and SW groups;
906 (k-l) Relative protein abundance of Histone H1.0B in FW and SW groups (k), including following *alkbh5a*
907 overexpression (l) All barcharts show mean ± S.D. (n=3), with significant differences from t-tests marked as:
908 *p<0.05, **p<0.01, ***p<0.001.
909
910 **Fig. 3 Hnrnpab1 is a reader protein that enhances the translation efficiency of *histone H1.0B*.** (a)
911 Experimental design for RNA pull-down and LC-MS/MS analysis to detect the potential reader proteins. The
912 positive and negative m^{6}A probes of *histone H1.0B* mRNA were designed and biosynthesized according to the
913 potential hyper-methylation sites; (b) Functional enrichment and interactome analysis of proteins showing
914 differential abundance, with top 20 enriched functional categories (by *P*-value) visualized; (c) Interactions
915 between proteins showing differential abundance and their corresponding functional categories; (d) Roles of

potential reader proteins drawn from the list showing differential abundance, according to published literature on different hnRNP family members; (e) Pie charts showing copy number and functional domains in hnRNPA/B gene family members across vertebrate species. Quarter segments within each pie signify a single gene copy, while a fully solid segment signifies four copies. Similarly, the presence of functional domains is indicated by solid segments in each pie chart; (f) Predicted binding relationships between hnRNPAB protein and m^{6}A residues in *histone H1.0B*; (g) Representative immunofluorescence staining images show the subcellular distribution of hnRNPAB proteins in gill of smolts from FW and SW groups. DAPI staining shows nuclei. Scale bar = 10 μm; (h) Relative expression of *hnrnpab1* between si-NC and si-*hnrnpab1* groups in RTgill-W1 cells; (i) Relative protein abundance of hnRNPAB1 and Histone H1.0B in RTgill-W1 cells transfected with si-NC or si-*hnrnpab1*. Gapdh was used as the loading control. All barcharts show mean ± S.D. (n=3), with significant differences from t-tests marked as: *p<0.05, **p<0.01, ***p<0.001.

Fig. 4 Chromatin remodeling in the gill of *O. mykiss* smolts challenged with seawater. (a) Distribution of ATAC-seq fragment lengths for FW and SW groups (n=3); (b) Signal enrichment of ATAC-seq data around transcription start sites (TSS) for FW and SW groups (n=3 merged per group); (c) Venn diagram showing open chromatin region sharing between FW and SW groups; (d) Top enriched gene sets of cell cycle from functional genes with uniquely open regions in FW group. FPKM was calculated to normalize the expression levels across RNA-seq samples in gill tissues of smolts under FW and SW groups; (e) Hierarchical clustering of cell cycle genes (rows) showing differential expression between FW and SW conditions (n=3, replicates shown in columns). The heatmap gradient from blue to red indicates low to high relative expression levels. The right panel shows the genomic locations of ATAC-seq peaks relative to these genes, with positions indicated along the gene body and flanking regions (−10 kb to +10 kb). Colors denote different genomic annotations, including promoter, exon, and

938 distal intergenic regions; (f) Transcription factor (TF) enrichment analysis of open chromatin regions specific to
939 the FW and SW groups. The point sizes and colors represent the enriched *P*-values; (g) Regulatory relationships
940 between enriched TF motifs and cell-cycle genes associated with FW-specific accessible chromatin regions. (h)
941 Dot plot showing the enriched KEGG pathways from genes with open chromatin regions specific to the SW group;
942 (i) Schematic representation of major nodes and functional genes in enriched Glioma and ErbB signaling pathways.
943 Red and cyan boxes indicate genes upregulated or downregulated in the SW group vs. FW group, respectively; (j)
944 Gene structure of four *tonebp* paralogs (*tonebpa1*, *tonebpa2*, *tonebpb1*, and *tonebpb2*) in *O. mykiss*, showing
945 coding sequences, conserved Pfam domains (RHD_DNA_bind), IPT domains, and introns; (k) Relative mRNA
946 expression of *tonebpa1* between FW and SW groups; (l-m) Relative mRNA expression levels of *tonebpa1* in
947 RTgill-W1 cells treated with inhibitors to ERK (l) or GSK3β (m) compared to controls. All barcharts show mean
948 ± S.D. (n=3), with significant differences from t-tests marked as: **p<0.01, ***p<0.001.
949
950 **Fig. 5 *tonebpa1* regulates the ionocyte cell cycle under hyperosmotic conditions.** (a) Dual-fluorescence *in situ*
951 hybridization shows that *tonebpa1* and *nka* mRNA co-localises in gill epithelium of smolts; (b) Schematic of
952 *tonebpa1* knockdown in RTgill-W1 cells, incorporating a salinity gradient challenge followed by RNA-seq and
953 flow cytometry analysis; (c) Comparisons of DEGs shared by or unique to si-NC-300 mOsm/L, si-*tonebpa1*-300
954 mOsm/L, si-NC-700 mOsm/L and si-*tonebpa1*-700 mOsm/L groups; (d) Regulatory relationships between
955 *tonebpa1* and its candidate target cell-cycle genes; (e) Dual-luciferase reporter assay for *tonebpa1* and three of its
956 candidate target genes; (f-g) Cell numbers and morphology of RTgill-W1 cell lines between si-NC and si-*tonebpa1*
957 groups under 300 mOsm/L ~ 1100 mOsm/L; (h) Representative flow cytometry results for cell viability, cell
958 apoptosis, and the cell cycle in RTgill-W1 cells of si-NC and si-*tonebpa1* groups; (i) FACS estimate of ionocyte
959 proportion within RTgill-W1 cells in the si-NC and si-*tonebpa1* groups under 700 mOsm/L conditions; (j) NKA

activity in ionocytes of RTgill-W1 cells transfected with si-NC and si-*tonebpa1* groups under 300 mOsm/L ~ 1100 mOsm/L conditions.

Fig 6 Proposed model for m^{6}A-dependent regulation of salinity adaptation and osmoregulation in gill epithelium of *O. mykiss* smolts. A diagram was performed to summarize our findings in this work. These results provided a conceptual advance to understand the roles of RNA m^{6}A methylation in re-modeling of chromatin accessibility and activation of *tonebpa1* gene. As proven, *tonebpa1* gene was specifically located in ionocytes of gill epithelium in *O. mykiss*. When confronting to hyper-osmotic seawater, it can participate in cell cycle regulation and maintain the normal proliferation of ionocytes, providing the strong support for osmoregulation and ensuring the successful adaptation to high-salinity seawater during migration in *O. mykiss* smolts.

Supplementary Files

This is a list of supplementary files associated with this preprint. Click to download.

- SupplementaryInformation.pdf
- SupplementaryData.zip